Analysis of Fractal-Fractional -Order Model of Tuberculosis with Vaccination and Treatment Interventions

Celestine Agbata Benedict[1]
Fabiana Çullhaj[2]
Emmanuel Abah[3]
Raimonda Dervishi[4]
William Obeng-Denteh[5]
Homan Emadifar[6]
Aseel Smerat[7]
Mbah Godwin Christopher Ezike[8]

[1]Department of Mathematics and Statistics, Faculty of Science, Confluence University ofScience and Technology, Osara, Nigeria
[2]Department of Mathematics, Faculty of Information Technology, Aleksandër Moisiu University of Durrës, Durrës, Albania
[3]Mathematical Sciences Department, Prince Abubakar Audu (formerly, Kogi State) University, Anyigba, Nigeria
[4]Department of Mathematical Engineering, Mathematical and Physical Engineering Faculty, Polytechnic University of Tirana, Tirana, Albania
[5]Department of Mathematics, College of Science, Kwame Nkrumah University of Science and Technology, Kumasi, Ghana
[6]Department of Mathematics, Saveetha School of Engineering, Saveetha Institute of Medical and Technical Sciences, Saveetha University, Chennai-602 105, Tamil Nadu, India; Department of Mathematics, Hamedan Branch, Islamic Azad University, Hamedan, Iran
[7]Hourani Center for Applied Scientific Research, Al-Ahliyya Amman University, Amman 19328, Jordan;
Department of Biosciences, Saveetha School of Engineering, Saveetha Institute of Medical and Technical Sciences, Chennai, 602105, India
[8]Department of Mathematics, Faculty of Physical Sciences, University of Nigeria, Nsukka, Nigeria

Received: 20 February 2026 | **Accepted:** 10 June 2026 | **Published:** 23 July 2026

© 2026 Agbata Benedict et al.

DOI: 10.56345/ijrdv13n237

Abstract

Tuberculosis (TB) remains a major global health challenge, particularly in regions with limited healthcare resources and high transmission environments. This study develops and analyzes a deterministic compartmental model of TB using fractal–fractional derivatives with Mittag-Leffler kernels, incorporating memory and hereditary effects that better reflect the disease's latent nature and long-term treatment outcomes. The total human population is stratified into seven classes: susceptible, vaccinated, exposed, acutely infected, chronically infected, treated, and recovered. The model explicitly integrates the influence of vaccination, treatment rates, immunity waning, and environmental interventions such as ventilation and sanitation improvements. Using fixed point theorems, we established the existence and uniqueness of model solutions, while positivity and boundedness analysis confirmed biological feasibility. Threshold conditions, including the basic reproduction number, were derived, and stability analysis for both disease-free and endemic equilibria was conducted. Sensitivity analysis revealed that parameters such as contact rate and exposure progression act as key drivers of disease spread, while vaccination, treatment, and environmental interventions effectively reduce the reproduction number. Numerical simulations using the Adams–Bashforth scheme demonstrated the dynamic effects of vaccination and treatment policies, showing significant reductions in susceptible and exposed populations as well as lower cumulative new cases under stronger intervention strategies. Data fitting with WHO TB incidence reports confirmed that the model aligns well with real-world observations.

Keywords: Tuberculosis (TB), Fractal–fractional derivatives, Data fitting, Sensitivity analysis, Numerical simulation

1. Introduction

Tuberculosis (TB), caused by *Mycobacterium tuberculosis*, remains among the deadliest infectious diseases globally. In 2023, approximately 10.8 million people contracted TB (95% uncertainty interval: 10.1–11.7 million) and about 1.25 million died**,** reaffirming TB as the leading infectious killer worldwide (World Health Organization, 2024; El Baz et al., 2024). A considerable portion of the global population harbors latent TB infection (LTBI), which serves as a reservoir for future active disease. A systematic review based on both IGRA and TST tests estimated the global prevalence of LTBI to be 24.8% (95% CI: 19.7–30.0%) and 21.2% (95% CI: 17.9–24.4%) respectively, indicating about one-quarter of the world's population is infected (Cohen et al., 2019). In the Middle East and North Africa, the prevalence of LTBI was even higher, averaging 41.8% (95% CI: 31.2–52.8%) among adults (Barry et al., 2021). The burden of TB remains concentrated in high-incidence areas. In 2023, 30 high-burden countries accounted for 87% of global incident cases, with India alone contributing 26%**,** followed by Indonesia, China, the Philippines, and Pakistan (WHO, 2024). Concurrently, MDR-TB poses rising concern: a meta-analysis covering Central and West Africa found a pooled MDR-TB treatment success rate of 74.6% (95% CI: 65.0–82.2%), higher than the global average but with wide variation across regions (Eshetie et al., 2018). Child TB is another pressing issue. TB incidence among children under 15 in the WHO European region increased by 10% in 2023, exceeding 7,500 reported cases the third consecutive annual increase reflecting persistent transmission and gaps in pediatric TB control (World Health Organization, 2025).

Nigeria continues to face one of the highest tuberculosis (TB) burdens globally, contributing substantially to Africa's case load (Daniel et al., 2006). Despite recent improvements in case notification, under-diagnosis remains a major challenge, with significant proportions of individuals never reaching formal health facilities (Adepoju et al., 2020). Pediatric TB has also emerged as a growing concern, with under-reporting contributing to hidden transmission reservoirs (Adejumo et al., 2016). Drug-resistant TB (DR-TB) complicates control efforts, with studies reporting rising prevalence in multiple Nigerian states, partly due to gaps in drug adherence and delayed diagnostics (Olusoji & Hassan, 2018). Furthermore, TB/HIV co-infection remains highly prevalent, with meta-analyses estimating co-infection rates above 25%, thereby intensifying morbidity and mortality risks (Balogun et al., 2020).

Agbata et al. (2025b) developed a six-compartment fractional-order model (susceptible, exposed/latent, acute, chronic, treated, recovered) to examine TB transmission while explicitly including delayed diagnosis and varying treatment efficacy. They used Caputo-type fractional derivatives and numerical schemes (Adams–Bashforth) to capture memory effects, performed sensitivity analysis, and showed that fractional orders produced slower decay in exposed/infected compartments (i.e., historical states influenced current dynamics). They concluded that fractional calculus better reflected TB's prolonged latency and treatment memory than integer-order models and highlighted parameters most impactful for control. Nandi et al. (2024) formulated a Caputo-Fabrizio fractional-order epidemiological model that incorporated vaccination, endogenous reactivation of latent infections, and exogenous reinfection. They derived reproduction numbers (R_0 , R_V), proved local stability and Ulam–Hyers stability properties, and used Adams–Bashforth numerical simulations with data fitting to validate model behavior against real data. They reported that inclusion of fractional dynamics produced trajectories that better matched empirical patterns and emphasized vaccination and reinfection as key drivers of long-term TB dynamics. Khan et al. (2024) proposed a fractal-fractional operator–based TB model (splitting populations into susceptible, drug-sensitive infected, multidrug-resistant infected, isolated, and recovered classes), established existence and uniqueness results, and analysed invariant regions and reproduction number. The authors proved Ulam–Hyers stability for the system and provided numerical solutions to illustrate how fractal-fractional dynamics influenced disease spread and control scenarios. They argued that fractal-fractional operators gave additional flexibility for capturing heterogeneous temporal patterns in TB transmission.

Abdo et al. (2025) developed an Atangana–Baleanu–Caputo fractional-order model to study co-

dynamics of tuberculosis and diabetes mellitus across susceptible, TB-infected, DM-infected, and co-infected compartments. They proved well-posedness (via the Banach fixed-point theorem), derived basic reproduction numbers for TB, DM and the co-system, and performed sensitivity analysis and numerical simulations (Adams–Bashforth) showing that lower fractional orders slowed disease decay. They validated parts of the model against short-term data and suggested fractional modelling as useful for capturing chronic co-existence effects. Avazzadeh et al. (2023) presented a fractional-order TB disease (FTBD) model in the Caputo sense and introduced an optimization/numerical method using generalized Laguerre polynomials and operational matrices to convert the fractional problem into a system of nonlinear algebraic equations. They simulated susceptible, exposed, untreated infected, treated infected, and recovered compartments and demonstrated that the GLP method produced accurate numerical approximations while enabling efficient parameter studies. They recommended the approach as a flexible numerical solver for fractional TB models

The aim of this study is to develop and analyze a fractal–fractional deterministic compartmental model that captures the transmission dynamics of tuberculosis (TB) under the influence of vaccination and environmental interventions. The model seeks to provide deeper insight into how fractional operators, which incorporate memory and hereditary properties, affect TB progression and control strategies. Specifically, the objectives are to investigate the role of vaccination in reducing the susceptible population, to assess the impact of environmental interventions on limiting disease transmission, and to evaluate the effects of treatment and immunity waning on long-term disease persistence. In addition, the study aims to derive threshold conditions such as the basic reproduction number, examine the stability of equilibrium states, and perform numerical simulations to demonstrate how fractional-order dynamics modify the spread of TB compared to classical integer-order models.

Tuberculosis (TB) continues to be a pressing global health challenge, especially in regions where healthcare systems face resource constraints and patients often experience delays in diagnosis or incomplete treatment. Traditional integer-order models have helped in understanding the disease dynamics, yet they do not fully capture the long memory and hereditary characteristics that are typical of TB's latent phase, treatment adherence, and the gradual loss of immunity. Although some studies have introduced fractional-order models to account for these features, they rarely include the role of environmental conditions, such as poor sanitation or overcrowding, which are known to facilitate TB transmission. Likewise, while vaccination and treatment have been widely studied in deterministic models, the combined influence of vaccination and environmental interventions within a fractional framework has not been comprehensively addressed. The present study seeks to bridge this gap by constructing a fractal–fractional model of TB transmission that integrates vaccination, treatment, immunity waning, and environmental interventions in a six-compartment structure. By employing fractal–fractional operators, the model incorporates both memory effects and complex temporal dynamics, offering a more realistic representation of TB spread than conventional approaches. This integrated perspective allows for a deeper assessment of long-term intervention strategies, including how vaccination programs and environmental improvements interact with treatment policies. The study contributes novel insights by deriving key thresholds, analyzing stability conditions, and demonstrating through numerical simulations how fractal–fractional dynamics influence TB control, thereby providing policymakers with a more robust framework for evaluating intervention effectiveness.

2. Methods

2.1 Model Formulation

A fully deterministic compartmental framework is developed to describe how tuberculosis spreads within a population. (TB) . The total human population is divided into six classes: susceptible humans (S_H), vaccinated humans (V_H), exposed humans (E_H), acutely infected humans (A_T), chronically

infected humans (C_T), treated humans (T_T), and recovered humans (R). Individuals are recruited into the susceptible class at a rate Λ_H . The effective contact rate β_T , combined with the probability of infection per contact, governs the transmission of TB from infectious to susceptible individuals. Progression from exposure to active TB infection occurs at the rate θ_T . Acutely infected humans progress to the chronic stage at a rate τ . Treatment is provided to both acutely and chronically infected individuals at rates γ_T and γ_C , respectively. Recovery from TB is achieved at a rate α_T . Natural mortality occurs at a rate μ_H , while TB-related mortality is represented by the disease-induced death rate δ_T and ς_T denotes immunity waning rate of partially immune humans. The vaccination rate which decreases the susceptible population is denoted by σ_T and the impact of environmental intervention is represented by ω . The model is built on several key assumptions to simplify the transmission dynamics of tuberculosis within the population. First, the total population is homogeneously mixed, meaning every individual has an equal probability of coming into contact with infectious individuals. Second, recruitment into the population occurs only through entry into the susceptible class, and all individuals are assumed to be born susceptible before any intervention such as vaccination. Third, individuals progress through disease stages in a sequential and well-defined manner, moving from exposure to acute infection, then possibly to chronic infection, treatment, and recovery, with fixed transition rates. Fourth, both natural death and disease-induced death are considered, but recovered individuals may lose partial immunity over time and return to a susceptible or partially susceptible state, reflecting waning immunity in the population.

2.2 The model equations

$$\begin{aligned}
\frac{dS_H}{dt} &= \Lambda_H + \varsigma_T R - \left((1-\omega)\lambda_T + \sigma_T + \mu_H\right) S_H \\
\frac{dV_H}{dt} &= \sigma_T S_H - \left(\psi_T + \mu_H\right) V_H \\
\frac{dE_T}{dt} &= (1-\omega)\lambda_T S_H + \psi_T V_H - \left(\theta_T + \mu_H\right) E_T \\
\frac{dA_T}{dt} &= \theta_T E_T - \left(\tau + \gamma_T + \delta_T + \mu_H\right) A_T \\
\frac{dC_T}{dt} &= \tau A_T - \left(\gamma_c + \delta_T + \mu_H\right) C_T \\
\frac{dT_T}{dt} &= \gamma_T A_T + \gamma_C C_T - \left(\alpha_T + \delta_T + \mu_H\right) T_T \\
\frac{dR}{dt} &= \alpha_T T_T - (\varsigma_T + \mu_H) R
\end{aligned} \qquad (1)$$

The force of infection for the Tuberculosis model is given as:

$$\lambda_T = \frac{\beta_T\left(\eta_1 A_T + \eta_2 C_T + \eta_3 T_T\right)}{N_H}$$

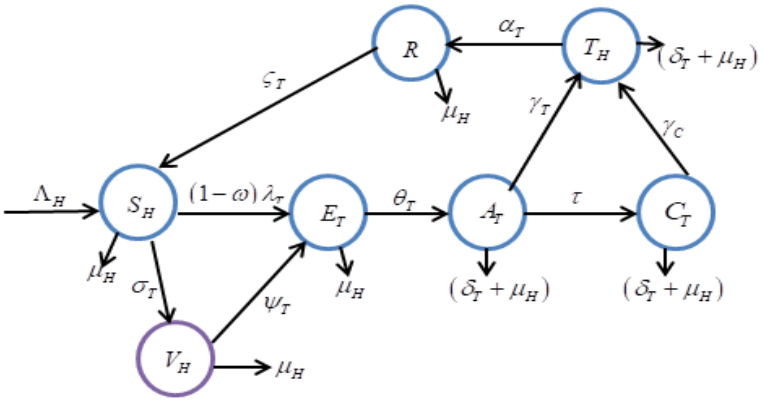

Figure 1. Schematic diagram for the TB Model

Figure 1 presents a simplified schematic of the tuberculosis (TB) transmission model, showing how individuals move between key epidemiological compartments (Agbata et al., 2025a, 2025c; Akowe et al., 2025). The model starts with the susceptible population, representing individuals who are at risk of infection.

Table 1. Description of variables and parameters.

Variable	Description
Susceptible humans	S_H
Vaccinated humans	V_H
Exposed Humans to TB	E_T
Acutely infected humans with TB	A_T
Chronically infected humans with TB .	C_T
Treated Humans to TB	T_T
Recovered Humans	R

Parameter	Description
Λ_H	Recruitment rate of humans
σ_T	Vaccination rate
ω	Environmental interventions
ς_T	Immunity waning rate of partially immune humans

Parameter	Description
θ_T	Progression rate of exposed TB to acutely infected TB class
β_H	Contact rate
ψ_T	Progression rate from vaccinated to exposed class
η_1, η_2, η_3	Modification parameters
μ_H	Natural death rate of humans
γ_T	Treatment rate of infected humans with TB
τ	Progression rate from acute TB to chronic TB class
δ_T	Disease induced death rate of infected acute TB , chronic TB
α_T	Recovery rate of infected individuals.

Table 1 provides an overview of the variables and parameters that form the foundation of the tuberculosis (TB) transmission model (Agbata et al., 2025a, 2025c). The variables represent the different human population compartments, including susceptible, vaccinated, exposed, acutely infected, chronically infected, treated, and recovered individuals (Agbata et al., 2025b; Akowe et al., 2025). This compartmental structure allows the model to capture the transitions between health states and the role of interventions such as vaccination and treatment.

2.3 Preliminaries

In this sections we present definitions, theorem and lemma used in the study. Let ϕ represent fractional-order while the symbol σ stands for fractal-dimension. When $x(t)$ remain continuous it also has fractal differentiability on (a,b) with σ, as presented by Atangana et al. (2020) and Rahman (2022).

Definition 1

The Caputo fractional differential operator makes use of the Mittag-Leffler Kernel to define the fractal fractional derivative of functions $x(t)$ in order ϕ while operating on dimension σ as the follows (Rahman, 2022):

$$FFHD_{0,t}^{\beta,\sigma} x(t) = \frac{AB(\beta)}{1-\beta} \int_a^t E_\beta \left[\frac{-\beta}{1-\beta} (t-s)^\beta \right] \frac{dy(s)}{dS^\sigma} ds, \quad t \geq a \geq 0, \tag{2}$$

Where

$\beta, \alpha \in (0,1], AB(\beta) = 1-\beta+\beta/\Gamma(\beta)$ is the normalization function with $AB(0) = AB(1) = 1$ and

$$d_x(t)/d_t\sigma = \lim_{S \to t} \left(x(s) - x(t) \right) / \left(s^\sigma - t^\sigma \right).$$

Moreover, the Mittag-Leffler function is defined by;

$$E_\beta(Z)=\sum_{k=0}^{\infty} Z^k\Gamma(\beta k+1), Z,\beta\in C,\beta>0,$$

with C is the set the of complex number.

Definition 2

The equation for fractal fractional integration with the Mittag-Leffler Kernel in the Caputo sense of order β for dimension σ (Rahman, 2022; Atangana et al., 2020):

$$FFHD_{0,t}^{\beta,\sigma}x(t)=\frac{\sigma(1-\beta)t^{\sigma-1}x(t)}{AB(\beta)}+\frac{\beta\sigma}{AB(\beta)}\int_a^t(t-s)^{\beta-1} S^{\beta-1}x(s)ds,\ t\geq a\geq 0. \tag{3}$$

Definition 3

$If\quad x\in C((a,b),R),$ the fractal Laplace transform of order β is given as follows (Rahman, 2022):

$$^{F}L_p^{\sigma}x(t)=\int_0^{\infty}x(t)\exp(-pt)t^{\sigma-1}dt$$

.

Lemma 1

Fractal fractional initial value problem is as follows (Atangana et al., 2020):

$$\begin{cases} FFHD_{0,t}^{\beta,\sigma}x(t)=G(t,x(t)),\ \ t\in[0,T],\beta,\sigma\in(0,1] \\ x(0)=x_0. \end{cases} \tag{5}$$

The problem in (5) can be expressed as (Qureshi et al., 2019):

$$\begin{cases} FFHD_{0,t}^{\beta,\sigma}x(t)=\sigma t^{\sigma-1}G(t,x(t)),\ \ t\in[0,T],\beta,\sigma\in(0,1] \\ x(0)=x_0. \end{cases} \tag{6}$$

The corresponding integral equation defines the solution of problem (5) is as follow:

$$x(t)=x(0)+\frac{\sigma t^{\sigma-1}(1-\beta)G(t,x(t))}{AB(\beta)}+\sigma\frac{\sigma\beta}{AB(\beta)\Gamma(\beta)}\int_0^t S^{\sigma-1}(t-s)^{\beta-1}G(S,x(s))dS. \tag{7}$$

Several Lemma became necessary for analyzing both uniqueness and existence in the proposed model.

Lemma 2

Banach fixed point theorem (Granas & Dugundji, 2003). The Banach space Y contains a closed subset $D\subset Y,\ D\neq 0$ within it. The operator P yields exactly one fixed point in D when it meets the contraction condition $P:D\to D$.

Lemma 3

Krasnoselskii's fixed point theorem (Krasnosel'skii, 1955). The set D consists of every element from Y forming both a non-empty subset and a closed as well as convex space.

Let P and Q represent the two operators such that,

$PU+QV\in D,$ whenever $U,V\in D,$

Q is compact and continuous

P denotes the contraction mapping. then, there exist $k\in D$ such $Z=PK+QK.$

The new application applied the fractal fractional derivative operator to advance the Tuberculosis

model (1) within the Mittag-Leffler Kernel framework $\beta \in (0,1]$ and $\sigma \in [0,1], FFHD_{0,t}^{\beta,\sigma}$, as follows;

$$\begin{aligned}
FFHD_{0,t}^{\beta,\sigma} S_H(t) &= G_1\left(t, S_H(t), V_H(t), E_T(t), A_T(t), C_T(t), T_T(t), R(t)\right),\\
FFHD_{0,t}^{\beta,\sigma} V_H(t) &= G_2\left(t, S_H(t), V_H(t), E_T(t), A_T(t), C_T(t), T_T(t), R(t)\right),\\
FFHD_{0,t}^{\beta,\sigma} E_T(t) &= G_3\left(t, S_H(t), V_H(t), E_T(t), A_T(t), C_T(t), T_T(t), R(t)\right),\\
FFHD_{0,t}^{\beta,\sigma} A_T(t) &= G_4\left(t, S_H(t), V_H(t), E_T(t), A_T(t), C_T(t), T_T(t), R(t)\right),\\
FFHD_{0,t}^{\beta,\sigma} C_T(t) &= G_5\left(t, S_H(t), V_H(t), E_T(t), A_T(t), C_T(t), T_T(t), R(t)\right),\\
FFHD_{0,t}^{\beta,\sigma} T_T(t) &= G_6\left(t, S_H(t), V_H(t), E_T(t), A_T(t), C_T(t), T_T(t), R(t)\right),\\
FFHD_{0,t}^{\beta,\sigma} R(t) &= G_7\left(t, S_H(t), V_H(t), E_T(t), A_T(t), C_T(t), T_T(t), R(t)\right).
\end{aligned} \tag{8}$$

Where $G_i = G_i\left(t, S_H(t), V_H(t), E_T(t), A_T(t), C_T(t), T_T(t), R(t)\right).$

The functions G_i of the developed model follow the sequence for i = 1, 2, 3,...,7 below;

$$\begin{aligned}
G_1 &= \Lambda_H + \varsigma_T R - \left((1-\omega)\lambda_T + \sigma_T + \mu_H\right) S_H,\\
G_2 &= \sigma_T S_H - \left(\psi_T + \mu_H\right) V_H,\\
G_3 &= (1-\omega)\lambda_T S_H + \psi_T V_H - \left(\theta_T + \mu_H\right) E_T,\\
G_4 &= \theta_T E_T - \left(\tau + \gamma_T + \delta_T + \mu_H\right) A_T,\\
G_5 &= \tau A_T - \left(\gamma_c + \delta_T + \mu_H\right) C_T,\\
G_6 &= \gamma_T A_T + \gamma_C C_T - \left(\alpha_T + \delta_T + \mu_H\right) T_T,\\
G_7 &= \alpha_T T_T - (\varsigma_T + \mu_H) R.
\end{aligned} \tag{9}$$

$$S_H(t) \geq 0, V_H(t) \geq 0, E_T(t) \geq 0, A_T(t) \geq 0, C_T(t) \geq 0, T_T(t) \geq 0, R(t) \geq 0.$$

The fractal fractional tuberculosis model exists under the label (8).

Let $\phi = 1$ in the FF-tuberculosis model transforms into the (7) to build an integer-order model system. The model is simplified into the fractional Tuberculosis model by letting $\sigma = 1$.

3. Results

3.1 Model Analysis

3.1.1 Positivity of the model solution

$$\left(R_+^7 = \left\{G \in R_+^7 : G \geq 0 \; and \left(S_H, V_H, E_T, A_T, C_T, T_T, R\right)^T\right\}\right)$$

The vector transform is expressed by $(.)^T$.

Theorem 1

G satisfies boundedness in R_+^7 in addition to being non-negative for the solution of the FF-Tuberculosis model described by equation (8).

Proof.

For $t \in (0, \infty)$, existence and uniqueness of the FF- Tuberculosis model (8) is obtained. Consequently, the non-negative region R_+^7 represents a positive invariant region according to the presented content. Our research used the FF- Tuberculosis model described in (8) as the basis for our analysis:

$$\begin{aligned}
&FFDH_{0,t}^{\beta,\sigma} S_H(t) = \Lambda_H + \varsigma_T R \geq 0,\\
&FFDH_{0,t}^{\beta,\sigma} V_H(t) = \sigma_T S_H \geq 0,\\
&FFDH_{0,t}^{\beta,\sigma} E_H(t) = (1-\omega)\lambda_T S_H + \psi_T V_H \geq 0,\\
&FFDH_{0,t}^{\beta,\sigma} A_T(t) = \theta_T E_T \geq 0,\\
&FFDH_{0,t}^{\beta,\sigma} C_T(t) = \tau A_T \geq 0,\\
&FFDH_{0,t}^{\beta,\sigma} T_T(t) = \gamma_T A_T + \gamma_C C_T \geq 0,\\
&FFDH_{0,t}^{\beta,\sigma} R(t) = \alpha_T T_T \geq 0.
\end{aligned} \tag{10}$$

If $\left(S_{H0}, V_{H0}, E_{T0}, A_{T0}, C_{T0}, T_{T0}, R_0\right) \in R_+^7$, then, from the time interval from (10) solution G remains prevented from escaping through the hyperplanes. Consequently, R_+^7 is a positively invariant:

$$N_H = S_H + V_H + E_T + A_T + C_T + T_T + R.$$

So from the FF- Tuberculosis model (8) we obtained:

$$\left\{FFHD_{0,t}^{\beta,\sigma} N_H(t) = \Lambda_H - \mu_H N_H\right\} \tag{11}$$

Using the fractal Laplace transform of Definition 2.3, we conclude that,

$$N_H(t) \leq \frac{\Lambda_H}{\mu_H} \; as \; t \to \infty.$$

So we now have the biological range of values of the FF-Tuberculosis model (8) as follows:

$$\left\{\left(S_H, V_H, E_T, A_T, C_T, T_T, R\right) \in R^7 : S_H, V_H, E_T, A_T, C_T, T_T, R \geq 0\right\}$$ and

$N_H(t) \leq \frac{\Lambda_H}{\mu_H}$.

This shows that the above model is biologically feasible.

3.2 Equilibrium points and their stabilities

The FF-Tuberculosis model demonstrates two steady states, which occur when the right side of equivalence (8) displays zero value. Then, we obtain:

3.3 The Disease free Equilibrium point

The disease-free equilibrium (DFE) represents the steady state where there is no infection, i.e. $E_T = A_T = C_T = T_T = R = 0$. This point reflects the complete absence of the disease within the population.

For the tuberculosis model, the DFE is given as:

$$E_0 = \left(S_H^0, V_H^0, E_T^0, A_T^0, C_T^0, T_T^0, R_T^0\right) = \left(\frac{\Lambda_H}{Q_1}, \frac{\sigma_T \Lambda_H}{\mu_H Q_1}, 0, 0, 0, 0, 0\right) \quad (12)$$

Where $Q_1 = \sigma_T + \mu_H$.

3.4 Basic Reproduction Number of the tuberculosis Model

The basic reproduction number (R_0) represents the average number of new infections caused by a single infectious individual in a fully susceptible population (Atokolo & Mbah, 2020). It serves as a critical threshold indicator: when R_0 is less than one, the disease eventually disappears, whereas values greater than one indicate that the infection can establish itself and continue to spread.

Let the matrices F and V be:

$$F = \begin{bmatrix} 0 & \frac{(1-\omega)\eta_1\mu_H}{Q_1} & \frac{(1-\omega)\eta_2\mu_H}{Q_1} & \frac{(1-\omega)\eta_3\mu_H}{Q_1} \\ 0 & 0 & 0 & 0 \\ 0 & 0 & 0 & 0 \\ 0 & 0 & 0 & 0 \end{bmatrix}, V = \begin{bmatrix} P_2 & 0 & 0 & 0 \\ -\theta_T & P_3 & 0 & 0 \\ 0 & -\tau & P_4 & 0 \\ 0 & -\gamma_T & -\gamma_C & P_5 \end{bmatrix}.$$

$$FV^{-1} = \begin{bmatrix} \frac{\theta_T(F_1P_4P_5 + F_2\tau P_5 + F_3P_4\gamma_T + F_3\tau\gamma_C)}{P_2P_3P_4P_5} & \frac{F_1P_4P_5 + F_2\tau P_5 + F_3P_4\gamma_T + F_3\tau\gamma_C}{P_4P_3P_5} & \frac{F_2}{P_4} + \frac{F_3\gamma_C}{P_4P_5} & \frac{F_3}{P_5} \\ 0 & 0 & 0 & 0 \\ 0 & 0 & 0 & 0 \\ 0 & 0 & 0 & 0 \end{bmatrix}$$

The inverse of V, denoted V^{-1}, is computed analytically or numerically. The next-generation

matrix is then obtained as $K = FV^{-1}$, and the basic reproduction number R_0 is the spectral radius (dominant eigenvalue) of K : $\mathrm{R}_0 = \rho(FV^{-1})$.

$$\frac{\theta_T\left(F_1P_4P_5 + F_2\tau P_5 + F_3P_4\gamma_T + F_3\tau\gamma_C\right)}{P_2P_3P_4P_5} \tag{13}$$

Where,

$$F_1 = \frac{(1-\omega)\eta_1\mu_H}{Q_1}, F_2 = \frac{(1-\omega)\eta_2\mu_H}{Q_1}, F_3 = \frac{(1-\omega)\eta_3\mu_H}{Q_1},$$

$$P_1 = (\psi_1 + \mu_H), P_2 = (\theta_T + \mu_H), P_3 = (\tau + \gamma_T + \delta_T + \mu_H), P_4 = (\gamma_C + \delta_T + \mu_H), P_5 = (\alpha_T + \delta_T + \mu_H),$$

$$P_6 = (\varsigma_T + \mu_H)$$

3.5 Endemic Equilibrium Point of the Tuberculosis Model

The endemic equilibrium point is the steady state where there is persistence or prevalence of disease in the population.

Theorem 2

The endemic equilibrium point of the Tuberculosis model is stable if $R_0 > 1$ and unstable if $R_0 < 1$

Proof.

To obtain the endemic equilibrium, we set the right-hand side of the differential equations to zero and solve for the state variables.

Thus, at the endemic equilibrium point:

$$\frac{dS_H}{dt} = \frac{dV_H}{dt} = \frac{dE_T}{dt} = \frac{dA_T}{dt} = \frac{dC_T}{dt} = \frac{dT_T}{dt} = \frac{dR}{dt} = 0$$

.

Let $\eta^* = (S_H^*, V_H^*, E_T^*, A_T^*, C_T^*, T_T^*, R^*)$ be the endemic equilibrium point.

Let's define:

$$W_1 = (\theta_T + \mu_H), \quad W_2 = (\tau + \gamma_T + \delta_T + \mu_H), \quad W_3 = (\gamma_c + \delta_T + \mu_H),$$

$$W_4 = (\alpha_T + \delta_T + \mu_H),$$

$$W_5 = (\varsigma_T + \mu_H), W_6 = (\psi_T + \mu_H), W_7 = ((1-\omega)\lambda_T + \sigma_T + \mu_H).$$

By making each compartment the subject of the formula when equated to zero, we obtain:

$$\text{At } \Lambda_H + \varsigma_T R^* - ((1-\omega)\lambda_T^* + \sigma_T + \mu_H)S_H^* = 0 \Rightarrow S_H^* = \frac{\Lambda_H + \varsigma_T R^*}{(1-\omega)\lambda_T^* + \sigma_T + \mu_H}$$

$$\text{At } \sigma_T S_H^* - (\psi_T + \mu_H)V_H^* = 0 \Rightarrow V_H^* = \frac{\sigma_T S_H^*}{W_6}$$

.

$$\text{At } (1-\omega)\lambda_T^* S_H^* + \psi_T V_H^* - (\theta_T + \mu_H)E_T^* = 0 \Rightarrow E_T^* = \frac{(1-\omega)\lambda_T^* S_H^* + \psi_T V_H^*}{W_1}$$

At $\theta_T E_T^* - (\tau + \gamma_T + \delta_T + \mu_H)A_T^* = 0 \Rightarrow A_T^* = \frac{\theta_T E_T^*}{W_2}$

At $\tau A_T^* - (\gamma_c + \delta_T + \mu_H)C_T^* = 0 \Rightarrow C_T^* = \frac{\tau A_T^*}{W_3}$

At $\gamma_T A_T^* + \gamma_C C_T^* - (\alpha_T + \delta_T + \mu_H)T_T^* = 0 \Rightarrow T_T^* = \frac{\gamma_T A_T^* + \gamma_C C_T^*}{W_4}$

At $\alpha_T T_T^* - (\varsigma_T + \mu_H)R^* = 0 \Rightarrow R^* = \frac{\alpha_T T_T^*}{W_5}$

Solving these equations in terms of each other.

R^* in terms of T_T^* using equation $R^* = \frac{\alpha_T T_T^*}{W_5}$

Substituting this into:

$$S_H^* = \frac{\Lambda_H + \varsigma_T \frac{\alpha_T T_T^*}{W_5}}{(1-\omega)\lambda_T^* + \sigma_T + \mu_H} = \frac{\Lambda_H W_5 + \varsigma_T \alpha_T T_T^*}{W_5((1-\omega)\lambda_T^{**} + \sigma_T + \mu_H)}, \quad V_H^* = \frac{\sigma_T S_H^*}{W_6},$$

$$E_T^* = \frac{(1-\omega)\lambda_T^* S_H^* + \psi_T V_H^{**}}{W_1}, \quad A_T^* = \frac{\theta_T E_T^*}{W_2}, \quad C_T^* = \frac{\tau A_T^*}{W_3}, \quad T_T^* = \frac{\gamma_T A_T^* + \gamma_C C_T^*}{W_4},$$

Now, let's substitute the force of infection:

$$\lambda_T^* = \frac{\beta_T(\eta_1 A_T^* + \eta_2 C_T^* + \eta_3 T_T^*)}{N_H^{**}}$$

After further substitutions, we have an equation for λ_T^* of the form:

$$\lambda_T^* = \frac{W_1 W_2 W_3 W_4 W_5 W_6 W_7 \mu_H (R_0 - 1)}{D}$$

Where,

$$D = (W_5 W_3 W_4(\theta_T + W_1) + W_1 W_5 W_3 W_4)\mu_H + W_5 W_3 \gamma_t \theta_t(\mu_h + \alpha_t) + W_5 \tau W_2 W_4(\mu_h + \gamma_k)$$

Thus, for λ_T^{**} to be positive at the endemic equilibrium point, we need $R_0 - 1 > 0 \Rightarrow R_0 > 1$ and the endemic equilibrium point is stable.

3.6 Sensitivity Analysis for the Tuberculosis Model

The sensitivity index of the reproduction number with respect to any parameter p is given by:

$$\Im_p^{R_0} = \frac{\partial R_0}{\partial p} \times \frac{p}{R_0}$$

$$\Im_{\beta_T}^{R_0}=1,\qquad \Im_{\theta_T}^{R_0}=1-\frac{\theta_T}{P_2},\qquad \Im_{\tau}^{R_0}=\frac{F_2P_5+F_3\gamma_C}{F_1P_4P_5+F_2\tau P_5+F_3P_4\gamma_T+F_3\tau\gamma_C}\cdot\tau,$$

$$\Im_{\gamma_T}^{R_0}=\frac{F_3P_4}{F_1P_4P_5+F_2\tau P_5+F_3P_4\gamma_T+F_3\tau\gamma_C}\cdot\gamma_T-\frac{\gamma_T}{P_3},\ \Im_{\alpha_T}^{R_0}=-\frac{\alpha_T}{P_5},\ \Im_{\omega}^{R_0}=-\frac{\omega}{1-\omega},$$

$$\Im_{\eta_1}^{R_0}=\frac{\eta_1F_1^{-1}\cdot F_1P_4P_5}{N}=\frac{\eta_1}{F_1}\cdot\frac{F_1P_4P_5}{N}=\frac{\eta_1P_4P_5}{N},\qquad \Im_{\eta_2}^{R_0}=\frac{\eta_2\tau P_5}{N},$$

$$\Im_{\eta_3}^{R_0}=\frac{\eta_3(P_4\gamma_T+\tau\gamma_C)}{N},\ \Im_{\sigma_T}^{R_0}=-\frac{\sigma_T}{Q_1},$$

$$\Im_{\gamma_C}^{R_0}=\frac{F_3\tau}{N}\cdot\gamma_C-\frac{\gamma_C}{P_4},\ \Im_{\psi_1}^{R_0}=-\frac{\psi_1}{P_1},$$

Where:

$$N=F_1P_4P_5+F_2\tau P_5+F_3P_4\gamma_T+F_3\tau\gamma_C$$

and

$$Q_1=\sigma_T+\mu_H,\quad P_1=\psi_1+\mu_H,\quad P_2=\theta_T+\mu_H,\quad P_3=\tau+\gamma_T+\delta_T+\mu_H,$$

$$P_4=\gamma_C+\delta_T+\mu_H,\quad P_5=\alpha_T+\delta_T+\mu_H$$

Substituting the values of the parameters into the expressions of the sensitivity analysis of the tuberculosis model above, we obtain the sensitivity indices of the model as presented below:

$$\Im_{\beta_T}^{R_0}=1,\quad \Im_{\theta_T}^{R_0}=0.999911,\quad \Im_{\tau}^{R_0}\approx 0.000732,\quad \Im_{\gamma_T}^{R_0}\approx 0.4333,\quad \Im_{\alpha_T}^{R_0}=-0.8261,$$

$$\Im_{\omega}^{R_0}=-0.6667,$$

$$\Im_{\eta_1}^{R_0}\approx 0.0253,\ \Im_{\eta_2}^{R_0}\approx 0.000146,\ \Im_{\eta_3}^{R_0}\approx 0.0243,\ \Im_{\sigma_T}^{R_0}=-0.8571,\ \Im_{\gamma_C}^{R_0}\approx -0.6313,$$

$$\Im_{\psi_1}^{R_0}=-0.99988.$$

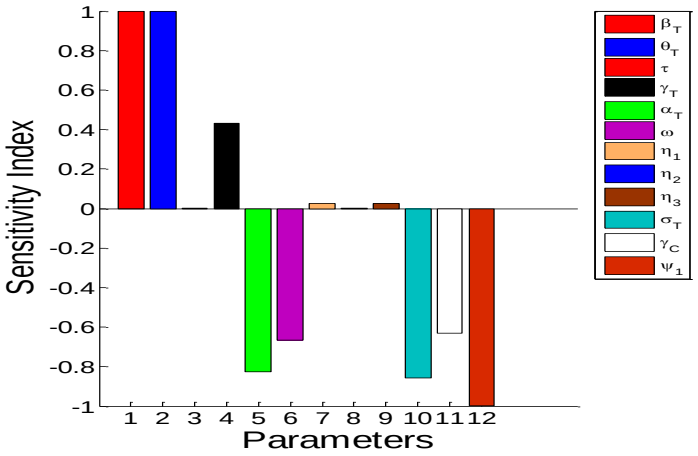

Figure 2a. Sensitivity bar chart

The sensitivity bar chart in Figure 2a shows that some parameters push tuberculosis transmission upward, while others help bring it down (Agbata et al., 2025c). For example, when the contact rate between susceptible and infected people is high, the basic reproduction number (R_0) rises. This means that TB spreads more easily in situations where people share crowded or poorly ventilated spaces, or where infection control is weak (Agbata et al., 2025a). Measures like patient isolation, better airflow, mask use, and cough etiquette can therefore help reduce R_0. The mathematical notation, equations, figures, and tables should also be carefully checked for consistency and formatting. On the other hand, factors such as treatment and environmental improvements work in the opposite direction, lowering R_0 when they are strengthened. Effective and timely treatment shortens the period when people remain infectious, prevents complications, and cuts down further transmission (Akowe et al., 2025). Ensuring access to reliable diagnostics, providing sufficient drug supplies, and supporting adherence through Directly Observed Therapy (DOT) all play a key role in this process. Similarly, environmental changes like improved housing, cleaner air, and especially natural ventilation in homes and health facilities reduce the chances of airborne TB spread.

3.7 Qualitative Analysis of the Fractal fractional Tuberculosis Model

For the FF- Tuberculosis model (10) to demonstrate its qualitative results we needs this specified Banach space. $\tau = [0,T]$ of all continuous real-valued functions denoted as; $Y = C(\tau \times R^7, R)$ equipped with the norm

$$\begin{aligned}
&\|x\| = \|S_H, V_H, E_H, A_T, C_T, T_T, R\| = \|S_H\| + \|V_H\| + \|E_H\| + \|A_T\| + \|C_T\| + \|T_T\| + \|R\|.\\
&\|S_H\| = Sup_{t\in\tau}|S_H(t)| = B_{h1},\\
&\|V_H\| = Sup_{t\in\tau}|V_H(t)| = B_{h2},\\
&\|E_H\| = Sup_{t\in\tau}|E_H(t)| = B_{h3},\\
&\|A_T\| = Sup_{t\in\tau}|A_T(t)| = B_{h4},\\
&\|C_T\| = Sup_{t\in\tau}|C_T(t)| = B_{h5},\\
&\|T_T\| = Sup_{t\in\tau}|T_T(t)| = B_{h6},\\
&\|R\| = Sup_{t\in\tau}|R(t)| = B_{h7}.
\end{aligned} \tag{14}$$

Where $(S_H, V_H, E_T, A_T, C_T, T_T, R) \in Y.$

$G \in Y$ *and* $x \in C(\tau, R)$, the FF- Tuberculosis model (8) can be expressed as:

$$\begin{cases} FFHD_{0,t}^{\beta,\sigma} x(t) = G(t, x(t)),\ t \in [0,T],\ \beta,\sigma \in (0,1] \\ x(0) = x_0 \end{cases} \tag{15}$$

$$x(t)=\begin{pmatrix} S_H(t)\\ V_H(t)\\ E_H(t)\\ A_T(t)\\ C_T(t)\\ T_T(t)\\ R(t)\end{pmatrix},\quad x(0)=\begin{pmatrix} S_H(0)\\ V_H(0)\\ E_H(0)\\ A_T(0)\\ C_T(0)\\ T_T(0)\\ R(0)\end{pmatrix},\qquad G(t,x(t))=\begin{pmatrix} G_1(t,S_H(t))\\ G_2(t,V_H(t))\\ G_3(t,E_H(t))\\ G_4(t,A_T(t))\\ G_5(t,C_T(t))\\ G_6(t,T_T(t))\\ G_7(t,R(t))\end{pmatrix}.$$

Where and (16)

The solution of problem (14) corresponds to this integral equation when $G_i, i=(1,2,...,7)$ are defined as (10);

$$x(t)=x(0)+\frac{\sigma t^{\sigma-1}(1-\beta)G(t,x(t))}{AB(\beta)}+\frac{\sigma\beta}{AB\beta\Gamma(\beta)}\int_0^t(t-s)^{\beta-1}G(s,x(s))ds \quad (17)$$

We simplify the calculations by introducing the following symbols in this work.

$$\begin{aligned}
&G_1(t,S_H(t))=G_1(t,S_H(t),V_H(t),E_T(t),A_T(t),C_T(t),T_T(t),R(t)),\\
&G_2(t,V_H(t))=G_2(t,S_H(t),V_H(t),E_T(t),A_T(t),C_T(t),T_T(t),R(t)),\\
&G_3(t,E_H(t))=G_3(t,S_H(t),V_H(t),E_T(t),A_T(t),C_T(t),T_T(t),R(t)),\\
&G_4(t,A_T(t))=G_4(t,S_H(t),V_H(t),E_T(t),A_T(t),C_T(t),T_T(t),R(t)),\\
&G_5(t,C_T(t))=G_5(t,S_H(t),V_H(t),E_T(t),A_T(t),C_T(t),T_T(t),R(t)),\\
&G_6(t,T_T(t))=G_6(t,S_H(t),V_H(t),E_T(t),A_T(t),C_T(t),T_T(t),R(t)),\\
&G_7(t,R(t))=G_7(t,S_H(t),V_H(t),E_T(t),A_T(t),C_T(t),T_T(t),R(t)).
\end{aligned} \quad (18)$$

The FF-Tuberculosis model (8) represents the following set of Volterra integral equations according to Lemma (1).

$$S_H(t)=S_H(0)+\frac{\sigma t^{\sigma-1}(1-\beta)G_1(t,S_H(t))}{AB(\beta)}+\frac{\sigma\beta}{AB(\beta)\Gamma(\beta)}\int_0^t S_H^{\sigma-1}(t-s)^{\beta-1}G_1(s,S_H(s))ds,$$

$$V_H(t)=V_H(0)+\frac{\sigma t^{\sigma-1}(1-\beta)G_2(t,V_H(t))}{AB(\beta)}+\frac{\sigma\beta}{AB(\beta)\Gamma(\beta)}\int_0^t S_H^{\sigma-1}(t-s)^{\beta-1}G_2(s,V_H(s))ds,$$

$$E_H(t)=E_H(0)+\frac{\sigma t^{\sigma-1}(1-\beta)G_3(t,E_H(t))}{AB(\beta)}+\frac{\sigma\beta}{AB(\beta)\Gamma(\beta)}\int_0^t E_H^{\sigma-1}(t-s)^{\beta-1}G_3(s,E_H(s))ds,$$

$$A_T(t)=A_T(0)+\frac{\sigma t^{\sigma-1}(1-\beta)G_4(t,A_T(t))}{AB(\beta)}+\frac{\sigma\beta}{AB(\beta)\Gamma(\beta)}\int_0^t A_T^{\sigma-1}(t-s)^{\beta-1}G_4(s,A_T(s))ds,$$

$$C_T(t)=C_T(0)+\frac{\sigma t^{\sigma-1}(1-\beta)G_5(t,C_T(t))}{AB(\beta)}+\frac{\sigma\beta}{AB(\beta)\Gamma(\beta)}\int_0^t C_T^{\sigma-1}(t-s)^{\beta-1}G_5(s,C_T(s))ds,$$

$$T_T(t)=T_T(0)+\frac{\sigma t^{\sigma-1}(1-\beta)G_6(t,T_T(t))}{AB(\beta)}+\frac{\sigma\beta}{AB(\beta)\Gamma(\beta)}\int_0^t T_T^{\sigma-1}(t-s)^{\beta-1}G_6(s,T_T(s))ds,$$

$$R(t)=R(0)+\frac{\sigma t^{\sigma-1}(1-\beta)G_7(t,R(t))}{AB(\beta)}+\frac{\sigma\beta}{AB(\beta)\Gamma(\beta)}\int_0^t R^{\sigma-1}(t-s)^{\beta-1}G_7(s,R(s))ds.$$

(19)

In view of (19), we define an operator,

$\tau: Y\to Y,$ where

$\tau=(\tau_1,\tau_2,\tau_3,\tau_4,\tau_5,\tau_6,\tau_7),$

$$(\tau_1,S_H)(t)=S_H(0)+\frac{\sigma t^{\sigma-1}(1-\beta)G_1(t,S_H(t))}{AB(\beta)}+\frac{\sigma\beta}{AB(\beta)\Gamma(\beta)}\int_0^t S_H^{\beta-1}(t-s)^{\beta-1}G_1(s,S_H(s))ds,$$

$$(\tau_1,V_H)(t)=V_H(0)+\frac{\sigma t^{\sigma-1}(1-\beta)G_2(t,V_H(t))}{AB(\beta)}+\frac{\sigma\beta}{AB(\beta)\Gamma(\beta)}\int_0^t V_H^{\beta-1}(t-s)^{\beta-1}G_2(s,V_H(s))ds,$$

$$(\tau_1,E_H)(t)=E_H(0)+\frac{\sigma t^{\sigma-1}(1-\beta)G_3(t,E_H(t))}{AB(\beta)}+\frac{\sigma\beta}{AB(\beta)\Gamma(\beta)}\int_0^t E_H^{\beta-1}(t-s)^{\beta-1}G_3(s,E_H(s))ds,$$

$$(\tau_1,A_T)(t)=A_T(0)+\frac{\sigma t^{\sigma-1}(1-\beta)G_4(t,A_T(t))}{AB(\beta)}+\frac{\sigma\beta}{AB(\beta)\Gamma(\beta)}\int_0^t A_T^{\beta-1}(t-s)^{\beta-1}G_4(s,A_T(s))ds,$$

$$(\tau_1,C_T)(t)=C_T(0)+\frac{\sigma t^{\sigma-1}(1-\beta)G_5(t,C_T(t))}{AB(\beta)}+\frac{\sigma\beta}{AB(\beta)\Gamma(\beta)}\int_0^t C_T^{\beta-1}(t-s)^{\beta-1}G_5(s,C_T(s))ds,$$

$$(\tau_1,T_T)(t)=T_T(0)+\frac{\sigma t^{\sigma-1}(1-\beta)G_6(t,T_T(t))}{AB(\beta)}+\frac{\sigma\beta}{AB(\beta)\Gamma(\beta)}\int_0^t T_T^{\beta-1}(t-s)^{\beta-1}G_6(s,T_T(s))ds,$$

$$(\tau_1,R)(t)=R(0)+\frac{\sigma t^{\sigma-1}(1-\beta)G_7(t,R(t))}{AB(\beta)}+\frac{\sigma\beta}{AB(\beta)\Gamma(\beta)}\int_0^t R^{\beta-1}(t-s)^{\beta-1}G_7(s,R(s))ds.$$

(20)

We transform the examined model into a fixed point problem for fixed point theory investigation. $(x=\tau x),$ This will apply to create a fixed theory.

Our next section demonstrates the FF-Tuberculosis model (8) achieves a single solution.

Theorem 3

Let $G\in Y$ satisfying the assumption below B_1 .

There exist a constant $L_{\max} = \max\{L_1, L_2, L_3, L_4, L_5, L_6, L_7\}$, such that,

$$\begin{vmatrix} G(t, S_H(t), V_H(t), E_T(t), A_T(t), C_T(t), T_T(t), R(t)) \\ -G(t, S_H^*(t), V_H^*(t), E_H^*(t), A_T^*(t), C_T^*(t), T_T^*(t), R^*(t)) \end{vmatrix}$$

$$\leq L_{\max} \begin{pmatrix} |S_H(t) - S_H^*(t)| + |V_H(t) - V_H^*(t)| + |E_H(t) - E_H^*(t)| . \\ + |A_T(t) - A_T^*(t)| + |C_T(t) - C_T^*(t)| + |T_T(t) - T_T^*(t)| \\ + |R(t) - R^*(t)| \end{pmatrix} \quad (21)$$

For any $S_H, V_H, E_H, A_T, C_T, T_T, B \in Y$ and $t \in \tau$.

Then, FF-Tuberculosis fever model (8) has a unique solution.

Proof.

Let D_{K1} be a bounded, closed and convex subset.

$$D = \left\{ (S_H, V_H, E_H, A_T, C_T, T_T, R) \in Y : \left\| (S_H, V_H, E_H, A_T, C_T, T_T, R) \right\| \leq K_1 \right\}$$

Where with a radius;

$$\left(\sigma(1-\beta) T_{\min^{\sigma-1}} + \frac{\phi T^{\beta+\sigma-1} \Gamma(\sigma+1)}{\Gamma(\sigma+1)} \right) \frac{L_{\max}}{AB(\beta)} < 1, \quad (22)$$

$$\frac{\rho_{\max} + \left(\sigma(1-\beta) T_{\min^{\sigma-1}} + \frac{\beta T^{\beta+\sigma-1} \Gamma(\sigma+1)}{\Gamma(\beta+\sigma)} \right) \frac{G_{\max^*}}{AB(\beta)}}{1 - \left(\sigma(1-\beta) T_{\min^{\alpha-1}} + \frac{\beta T^{\beta+\sigma-1} \Gamma(\sigma+1)}{\Gamma(\beta+\sigma)} \right) \frac{L_{\max^*}}{AB(\beta)}}$$

Where $\rho_{\max} = \max\{S_{H0}, V_{H0}, E_{H0}, A_{T0}, C_{T0}, T_{T0}, R_0\}$,

$G_{\max^*} = \max\{G_1^*, G_2^*, G_3^*, G_4^*, G_5^*, G_6^*, G_7^*\}$,

and let

$Sup_{t \in \tau} |G_i(s, 0)| = G_i^* < +\infty,\ i = 1, 2, 3, 4, 5, 6, 7.$

First we show that, $\tau D_{K1} \subset D_{K1}$.

For any $(S_H, V_H, E_H, A_T, C_T, T_T, R) \in D_{K1}, t \in \tau,$

we obtained that,

$$\left|\left(\tau_1 S_H\right)(t)\right| \leq \left|S_H(0)\right| + \sigma t^{\beta-1}(1-\beta)\left|G_1,\left(t,S_H(t)\right)\right| + \frac{\beta\sigma}{AB(\beta)\Gamma(\beta)}\int_0^t S_H^{\sigma-1}(t-s)^{\beta-1}\left|G_1\left(s,S_H(s)\right)\right|ds,$$

$$\leq \left|S_H(0)\right| + \frac{\sigma t^{\beta-1}(1-\beta)}{AB(\beta)}\left[L_1\left(\left|S_H(t)\right|+\left|V_H(t)\right|+\left|E_H(t)\right|+\left|A_T(t)\right|+\left|C_T(t)\right|+\left|T_T(t)\right|+\left|R(t)\right|\right)+G_1^*\right]$$

$$+\frac{\beta\sigma}{AB(\beta)\Gamma(\beta)}\int_0^t S^{\sigma-1}(t-s)^{\phi-1}\left[\begin{matrix}L_1\left(\left|S_H(s)\right|+\left|V_H(s)\right|+\left|E_H(s)\right|+\left|A_T(s)\right|+\left|C_T(s)\right|+\left|T_T(s)\right|+\left|R(s)\right|\right)\\ +G_1^*\end{matrix}\right]ds, \tag{23}$$

$$\leq S_{H0} + \left(\frac{\sigma(1-\beta)T_{\min^{\sigma-1}}}{AB(\beta)} + \frac{\sigma T^{\beta+\sigma-1}\Gamma(\sigma+1)}{AB(\beta)\Gamma(\beta+\sigma)}\right)$$

$$\left[L_1\left(\left\|S_H\right\|+\left\|V_H\right\|+\left\|E_H\right\|+\left\|A_T\right\|+\left\|C_T\right\|+\left\|T_T\right\|+\left\|R\right\|\right)+G_1^*\right].$$

We now obtain:

$$\left\|\tau_1 S_H\right\| \leq S_{H0} + \left(\frac{\sigma(1-\beta)T_{\min^{\sigma-1}}}{AB(\beta)} + \frac{\beta T^{\beta+\sigma-1}\Gamma(\sigma+1)}{AB(\beta)\Gamma(\beta+\sigma)}\right)\left[L_1K_1+G_1^*\right], \tag{24}$$

Similarly, we have

$$\left\|\tau_2 V_H\right\| \leq V_{H0} + \left(\frac{\sigma(1-\beta)T_{\min^{\sigma-1}}}{AB(\beta)} + \frac{\beta T^{\beta+\sigma-1}\Gamma(\sigma+1)}{AB(\beta)\Gamma(\beta+\sigma)}\right)\left[L_2K_2+G_2^*\right],$$

$$\left\|\tau_3 E_H\right\| \leq E_{H0} + \left(\frac{\sigma(1-\beta)T_{\min^{\sigma-1}}}{AB(\beta)} + \frac{\beta T^{\beta+\sigma-1}\Gamma(\sigma+1)}{AB(\beta)\Gamma(\beta+\sigma)}\right)\left[L_3K_3+G_3^*\right],$$

$$\left\|\tau_4 A_T\right\| \leq A_{T0} + \left(\frac{\sigma(1-\beta)T_{\min^{\sigma-1}}}{AB(\beta)} + \frac{\beta T^{\beta+\sigma-1}\Gamma(\sigma+1)}{AB(\beta)\Gamma(\beta+\sigma)}\right)\left[L_4K_4+G_4^*\right],$$

$$\left\|\tau_5 C_T\right\| \leq C_{T0} + \left(\frac{\sigma(1-\beta)T_{\min^{\sigma-1}}}{AB(\beta)} + \frac{\beta T^{\beta+\sigma-1}\Gamma(\sigma+1)}{AB(\beta)\Gamma(\beta+\sigma)}\right)\left[L_5K_5+G_5^*\right],$$

$$\left\|\tau_5 T_T\right\| \leq T_{T0} + \left(\frac{\sigma(1-\beta)T_{\min^{\sigma-1}}}{AB(\beta)} + \frac{\beta T^{\beta+\sigma-1}\Gamma(\sigma+1)}{AB(\beta)\Gamma(\beta+\sigma)}\right)\left[L_6K_6+G_6^*\right],$$

$$\left\|\tau_7 R\right\| \leq R_0 + \left(\frac{\sigma(1-\beta)T_{\min^{\sigma-1}}}{AB(\beta)} + \frac{\beta T^{\beta+\sigma-1}\Gamma(\sigma+1)}{AB(\beta)\Gamma(\beta+\sigma)}\right)\left[L_7K_7+G_7^*\right], \tag{25}$$

From (24) - (25), it implies that, $\tau D_{K1} \subset DK_{K1}$.

Secondly, we show that τ is a contraction.

We assume that,

$\left(S_H, V_H, E_H, A_T, C_T, T_T, R\right) \in D_{K1}$ and $\left(S_H^*, V_H^*, E_H^*, A_T^*, C_T^*, T_T^*, R^*\right) \in D_{K1}$

We have:

$$\left|\left(\tau_1 S_H\right)(t) - \left(\tau_1 S_H^*\right)(t)\right|$$

$$\leq \frac{\sigma t^{\sigma-1}(1-\beta)}{AB(\beta)}\left|G_1\left(t, S_H(t) - G_1\left(t, S_H^*(t)\right)\right)\right| + \frac{\sigma\beta}{AB(\beta)\Gamma(\beta)}\int_0^t S_H^{\sigma-1}(t-s)^{\beta-1}\left|G_1\left(s, S_H(s) - G_1\left(s, S_H^*(s)\right)\right)\right| ds,$$

$$\leq \frac{\sigma t^{\sigma-1}(1-\beta)}{AB(\beta)}\left[L_1\left(\begin{array}{l}\left|S_H(t) - S_H^*(t)\right| + \left|V_H(t) - V_H^*(t)\right| + \left|E_H(t) - E_H^*(t)\right| + \left|A_T(t) - A_T^*(t)\right| + \left|C_T(t) - C_T^*(t)\right| \\ + \left|T_T(t) - T_T^*(t)\right| + \left|R(t) - R^*(t)\right|\end{array}\right)\right]$$

$$+ \frac{\sigma\beta}{AB(\beta)\Gamma(\beta)}\int_0^t S^{\sigma-1}(t-s)^{\beta-1}\left[L_1\left(\begin{array}{l}\left|S_H(t) - S_H^*(t)\right| + \left|V_H(t) - V_H^*(t)\right| + \left|E_H(t) - E_H^*(t)\right| + \left|A_T(t) - A_T^*(t)\right| \\ + \left|C_T(t) - C_T^*(t)\right| + \left|T_T(t) - T_T^*(t)\right| + \left|R(t) - R^*(t)\right|\end{array}\right)\right].$$

$$\leq \left(\frac{\sigma(1-\beta)T_{\min^{\sigma-1}}}{AB(\beta)} + \frac{\phi T^{\beta+\sigma-1} + \Gamma(\sigma+1)}{\Gamma(\sigma+\beta)}\right)\frac{L_1}{AB(\beta)}\left(\begin{array}{l}\left\|S_H(t) - S_H^*(t)\right\| + \left\|V_H(t) - V_H^*(t)\right\| + \left\|E_H(t) - E_H^*(t)\right\| \\ + \left\|A_T(t) - A_T^*(t)\right\| + \left\|C_T(t) - C_T^*(t)\right\| + \left\|T_T(t) - T_T^*(t)\right\| \\ + \left\|R(t) - R^*(t)\right\|\end{array}\right). \tag{26}$$

Then,

$$\left|\begin{array}{l}\left(\tau_1 S_H\right)(t) \\ -\left(\tau_1 S_H^*\right)(t)\end{array}\right| \leq \left(\frac{\sigma(1-\beta)T_{\min^{\sigma-1}}}{AB(\beta)} + \frac{\beta T^{\beta+\sigma-1} + \Gamma(\sigma+1)}{\Gamma(\sigma+\beta)}\right)\frac{L_1}{AB(\beta)}\left(\begin{array}{l}\left\|S_H(t) - S_H^*(t)\right\| + \left\|V_H(t) - V_H^*(t)\right\| \\ + \left\|E_H(t) - E_H^*(t)\right\| + \left\|A_T(t) - A_T^*(t)\right\| \\ + \left\|C_T(t) - C_T^*(t)\right\| + \left\|T_T(t) - T_T^*(t)\right\| \\ + \left\|R(t) - R^*(t)\right\|\end{array}\right).$$

Similarly, we have:

$$\left|\begin{array}{l}\left(\tau_2 V_H\right)(t) \\ -\left(\tau_2 V_H^*\right)(t)\end{array}\right| \leq \left(\frac{\sigma(1-\beta)T_{\min^{\sigma-1}}}{AB(\beta)} + \frac{\beta T^{\beta+\sigma-1} + \Gamma(\sigma+1)}{\Gamma(\sigma+\beta)}\right)\frac{L_2}{AB(\beta)}\left(\begin{array}{l}\left\|S_H(t) - S_H^*(t)\right\| + \left\|V_H(t) - V_H^*(t)\right\| \\ + \left\|E_H(t) - E_H^*(t)\right\| + \left\|A_T(t) - A_T^*(t)\right\| \\ + \left\|C_T(t) - C_T^*(t)\right\| + \left\|T_T(t) - T_T^*(t)\right\| \\ + \left\|R(t) - R^*(t)\right\|\end{array}\right).$$

$$\left|\begin{array}{l}\left(\tau_3 E_H\right)(t) \\ -\left(\tau_3 E_H^*\right)(t)\end{array}\right| \leq \left(\frac{\sigma(1-\beta)T_{\min^{\sigma-1}}}{AB(\beta)} + \frac{\beta T^{\beta+\sigma-1} + \Gamma(\sigma+1)}{\Gamma(\sigma+\beta)}\right)\frac{L_3}{AB(\beta)}\left(\begin{array}{l}\left\|S_H(t) - S_H^*(t)\right\| + \left\|V_H(t) - V_H^*(t)\right\| \\ + \left\|E_H(t) - E_H^*(t)\right\| + \left\|A_T(t) - A_T^*(t)\right\| \\ + \left\|C_T(t) - C_T^*(t)\right\| + \left\|T_T(t) - T_T^*(t)\right\| \\ + \left\|R(t) - R^*(t)\right\|\end{array}\right).$$

$$\left|\begin{array}{l}\left(\tau_4 A_T\right)(t) \\ -\left(\tau_4 A_T^*\right)(t)\end{array}\right| \leq \left(\frac{\sigma(1-\beta)T_{\min^{\sigma-1}}}{AB(\beta)} + \frac{\beta T^{\beta+\sigma-1} + \Gamma(\sigma+1)}{\Gamma(\sigma+\beta)}\right)\frac{L_4}{AB(\beta)}\left(\begin{array}{l}\left\|S_H(t) - S_H^*(t)\right\| + \left\|V_H(t) - V_H^*(t)\right\| \\ + \left\|E_H(t) - E_H^*(t)\right\| + \left\|A_T(t) - A_T^*(t)\right\| \\ + \left\|C_T(t) - C_T^*(t)\right\| + \left\|T_T(t) - T_T^*(t)\right\| \\ + \left\|R(t) - R^*(t)\right\|\end{array}\right).$$

$$\left|\begin{array}{l}\left(\tau_5 C_T\right)(t) \\ -\left(\tau_5 C_T^*\right)(t)\end{array}\right| \leq \left(\frac{\sigma(1-\beta)T_{\min^{\sigma-1}}}{AB(\beta)} + \frac{\beta T^{\beta+\sigma-1} + \Gamma(\sigma+1)}{\Gamma(\sigma+\beta)}\right)\frac{L_5}{AB(\beta)}\left(\begin{array}{l}\left\|S_H(t) - S_H^*(t)\right\| + \left\|V_H(t) - V_H^*(t)\right\| \\ + \left\|E_H(t) - E_H^*(t)\right\| + \left\|A_T(t) - A_T^*(t)\right\| \\ + \left\|C_T(t) - C_T^*(t)\right\| + \left\|T_T(t) - T_T^*(t)\right\| \\ + \left\|R(t) - R^*(t)\right\|\end{array}\right).$$

$$\left|\begin{matrix}(\tau_6 T_T)(t)\\ -(\tau_6 T_T^*)(t)\end{matrix}\right| \le \left(\frac{\sigma(1-\beta)T_{\min^{\sigma-1}}}{AB(\beta)} + \frac{\beta T^{\beta+\sigma-1}+\Gamma(\sigma+1)}{\Gamma(\sigma+\beta)}\right)\frac{L_6}{AB(\beta)}\begin{pmatrix}\|S_H(t)-S_H^*(t)\|+\|V_H(t)-V_H^*(t)\|\\ +\|E_H(t)-E_H^*(t)\|+\|A_T(t)-A_T^*(t)\|\\ +\|C_T(t)-C_T^*(t)\|+\|T_T(t)-T_T^*(t)\|\\ +\|R(t)-R^*(t)\|\end{pmatrix}.$$

$$\left|\begin{matrix}(\tau_7 R)(t)\\ -(\tau_6 R^*)(t)\end{matrix}\right| \le \left(\frac{\sigma(1-\beta)T_{\min^{\sigma-1}}}{AB(\beta)} + \frac{\beta T^{\beta+\sigma-1}+\Gamma(\sigma+1)}{\Gamma(\sigma+\beta)}\right)\frac{L_7}{AB(\beta)}\begin{pmatrix}\|S_H(t)-S_H^*(t)\|+\|V_H(t)-V_H^*(t)\|\\ +\|E_H(t)-E_H^*(t)\|+\|A_T(t)-A_T^*(t)\|\\ +\|C_T(t)-C_T^*(t)\|+\|T_T(t)-T_T^*(t)\|\\ +\|R(t)-R^*(t)\|\end{pmatrix}. \quad (27)$$

Since

$\tau = (\tau_1, \tau_2, \tau_3, \tau_4, \tau_5, \tau_6, \tau_7)$ *and* $L_{\max} > 0$

with the result obtained from (26)-(27) , we have;

$$\left\|\tau(S_H, V_H, E_H, A_T, C_T, T_T, R) - \tau(S_H^*, V_H^*, E_H^*, A_T^*, C_T^*, T_T^*, R^*)\right\|,$$

$$\le \left(\frac{\sigma(1-\beta)T_{\min^{\sigma-1}}}{AB(\beta)} + \frac{\phi T^{\beta+\sigma-1}+\Gamma(\sigma+1)}{\Gamma(\sigma+\beta)}\right)\frac{L_{\max}}{AB(\beta)}\begin{pmatrix}\|S_H(t)-S_H^*(t)\|+\|V_H(t)-V_H^*(t)\|\\ +\|E_H(t)-E_H^*(t)\|+\|A_T(t)-A_T^*(t)\|\\ +\|C_T(t)-C_T^*(t)\|+\|T_T(t)-T_T^*(t)\|\\ +\|R(t)-R^*(t)\|\end{pmatrix}.$$

By the condition (22), then τ is a contraction.

Lemma 2 establishes that model (8) of FF-Tuberculosis has a solution.

Theorem 4

Let $G \in Y$ satisfying the assumptions (B_1) in theorem 3 and (B_1) there exist constants, $g_{i,j} > 0, i = 0,1,2,...,7$, $j = 0,1,2,...,7$ such that:

$$\left|G(t, S_H(t), V_H(t), E_H(t), A_T(t), C_T(t), T_T(t), R(t))\right| \quad (28)$$

$$\le g_{0j} + g_{1j}\left|S_H(t)\right| + g_{2j}\left|V_H(t)\right| + g_{3j}\left|E_H(t)\right| + g_{4j}\left|A_T(t)\right| + g_{5j}\left|C_T(t)\right| + g_{6j}\left|T_T(t)\right| + g_{7j}\left|R(t)\right|. \quad (29)$$

If $\sigma(1-\phi)T_{\min^{\sigma-1}} L_{\max} L_{AB(\phi)}$.

Then, the FF- Tuberculosis model (8) has at least one solution.

Proof.

We define a set

$$D_{K2} = \left\{(S_H, V_H, E_H, A_T, C_T, A_T, R) \in Y : \left\|(S_H, V_H, E_H, A_T, C_T, A_T, R)\right\| \le K_2\right\}.$$

Applying the above equations, we can define two operators $(Q, P): D_{K2} \to Y$

$Q = (Q_1, Q_2, Q_3, Q_4, Q_5, Q_6, Q_7)$ and $P = (P_1, P_2, P_3, P_4, P_5, P_6, P_7)$.

The operator Q is defined by;

$$\left(Q_1, S_H\right)(t) = S_H(0) + \frac{\sigma t^{\sigma-1}(1-\beta) G_1\left(t, S_H(t)\right)}{AB(\beta)},$$
$$\left(Q_2, V_H\right)(t) = V_H(0) + \frac{\sigma t^{\sigma-1}(1-\beta) G_2\left(t, V_H(t)\right)}{AB(\beta)},$$
$$\left(Q_3, E_H\right)(t) = E_H(0) + \frac{\sigma t^{\sigma-1}(1-\beta) G_3\left(t, E_H(t)\right)}{AB(\beta)},$$
$$\left(Q_4, A_T\right)(t) = A_T(0) + \frac{\sigma t^{\sigma-1}(1-\beta) G_4\left(t, A_T(t)\right)}{AB(\beta)},$$
$$\left(Q_5, C_T\right)(t) = C_T(0) + \frac{\sigma t^{\sigma-1}(1-\beta) G_5\left(t, A_T(t)\right)}{AB(\beta)},$$
$$\left(Q_6, A_T\right)(t) = A_T(0) + \frac{\sigma t^{\sigma-1}(1-\beta) G_6\left(t, A_T(t)\right)}{AB(\beta)},$$
$$\left(Q_7, R\right)(t) = R(0) + \frac{\sigma t^{\sigma-1}(1-\beta) G_7\left(t, R(t)\right)}{AB(\beta)}, \tag{30}$$

And the operator P is defined by:

$$\left(P_1, S_H\right)(t) = \frac{\sigma\beta}{AB(\beta)\Gamma(\beta)} \int_0^t S^{\sigma-1}(t-s)^{\beta-1} G_1\left(s, S_H(t)\right) ds,$$
$$\left(P_2, V_H\right)(t) = \frac{\sigma\beta}{AB(\beta)\Gamma(\beta)} \int_0^t S^{\sigma-1}(t-s)^{\beta-1} G_2\left(s, V_H(t)\right) ds,$$
$$\left(P_3, E_H\right)(t) = \frac{\sigma\beta}{AB(\beta)\Gamma(\beta)} \int_0^t S^{\sigma-1}(t-s)^{\beta-1} G_3\left(s, E_H(t)\right) ds,$$
$$\left(P_4, A_T\right)(t) = \frac{\sigma\beta}{AB(\beta)\Gamma(\beta)} \int_0^t S^{\sigma-1}(t-s)^{\beta-1} G_4\left(s, A_T(t)\right) ds,$$
$$\left(P_5, C_T\right)(t) = \frac{\sigma\beta}{AB(\beta)\Gamma(\beta)} \int_0^t S^{\sigma-1}(t-s)^{\beta-1} G_5\left(s, C_T(t)\right) ds,$$
$$\left(P_6, T_T\right)(t) = \frac{\sigma\beta}{AB(\beta)\Gamma(\beta)} \int_0^t S^{\sigma-1}(t-s)^{\beta-1} G_6\left(s, T_T(t)\right) ds,$$
$$\left(P_7, R\right)(t) = \frac{\sigma\beta}{AB(\beta)\Gamma(\beta)} \int_0^t S^{\sigma-1}(t-s)^{\beta-1} G_6\left(s, R(t)\right) ds. \tag{31}$$

Using (B_1) in theorem 3, for any

$(S_H, V_H, E_H, A_T, C_T, T_T, R) \in D_{K1}$ and $(S_H^*, V_H^*, E_H^*, A_T^*, C_T^*, T_T^*, R^*) \in D_{K1}$

$$\left\|Q_1 S_H - Q_1 S_H^*\right\| \le \frac{\sigma(1-\beta) T_{\min^{\sigma-1}}}{AB(\beta)} Sup\left|G_1(t, S_H(t)) - G_1(t, S_H^*(t))\right|,$$

$$\left\|Q_1 S_H - Q_1 S_H^*\right\| \le \frac{\sigma(1-\beta) T_{\min^{\sigma-1}}}{AB(\beta)} L_1 \begin{pmatrix} \left\|S_H - S_H^*\right\| + \left\|V_H - V_H^*\right\| + \left\|E_H - E_H^*\right\| + \left\|A_T - A_T^*\right\| \\ + \left\|C_T - C_T^*\right\| + \left\|T_T - T_T^*\right\| + \left\|R - R^*\right\| \end{pmatrix},$$

$$\left\|Q_2 V_H - Q_2 V_H^*\right\| \le \frac{\sigma(1-\beta) T_{\min^{\sigma-1}}}{AB(\beta)} L_2 \begin{pmatrix} \left\|S_H - S_H^*\right\| + \left\|V_H - V_H^*\right\| + \left\|E_H - E_H^*\right\| + \left\|A_T - A_T^*\right\| \\ + \left\|C_T - C_T^*\right\| + \left\|T_T - T_T^*\right\| + \left\|R - R^*\right\| \end{pmatrix},$$

$$\left\|Q_3 E_H - Q_3 E_H^*\right\| \le \frac{\sigma(1-\beta) T_{\min^{\sigma-1}}}{AB(\beta)} L_3 \begin{pmatrix} \left\|S_H - S_H^*\right\| + \left\|V_H - V_H^*\right\| + \left\|E_H - E_H^*\right\| + \left\|A_T - A_T^*\right\| \\ + \left\|C_T - C_T^*\right\| + \left\|T_T - T_T^*\right\| + \left\|R - R^*\right\| \end{pmatrix},$$

$$\left\|Q_4 A_T - Q_4 A_T^*\right\| \le \frac{\sigma(1-\beta) T_{\min^{\sigma-1}}}{AB(\beta)} L_4 \begin{pmatrix} \left\|S_H - S_H^*\right\| + \left\|V_H - V_H^*\right\| + \left\|E_H - E_H^*\right\| + \left\|A_T - A_T^*\right\| \\ + \left\|C_T - C_T^*\right\| + \left\|T_T - T_T^*\right\| + \left\|R - R^*\right\| \end{pmatrix},$$

$$\left\|Q_5 C_T - Q_5 C_T^*\right\| \le \frac{\sigma(1-\beta) T_{\min^{\sigma-1}}}{AB(\beta)} L_5 \begin{pmatrix} \left\|S_H - S_H^*\right\| + \left\|V_H - V_H^*\right\| + \left\|E_H - E_H^*\right\| + \left\|A_T - A_T^*\right\| \\ + \left\|C_T - C_T^*\right\| + \left\|T_T - T_T^*\right\| + \left\|R - R^*\right\| \end{pmatrix},$$

$$\left\|Q_6 T_T - Q_6 T_T^*\right\| \le \frac{\sigma(1-\beta) T_{\min^{\sigma-1}}}{AB(\beta)} L_6 \begin{pmatrix} \left\|S_H - S_H^*\right\| + \left\|V_H - V_H^*\right\| + \left\|E_H - E_H^*\right\| + \left\|A_T - A_T^*\right\| \\ + \left\|C_T - C_T^*\right\| + \left\|T_T - T_T^*\right\| + \left\|R - R^*\right\| \end{pmatrix},$$

$$\left\|Q_7 R - Q_7 R^*\right\| \le \frac{\sigma(1-\beta) T_{\min^{\sigma-1}}}{AB(\beta)} L_7 \begin{pmatrix} \left\|S_H - S_H^*\right\| + \left\|V_H - V_H^*\right\| + \left\|E_H - E_H^*\right\| + \left\|A_T - A_T^*\right\| \\ + \left\|C_T - C_T^*\right\| + \left\|T_T - T_T^*\right\| + \left\|R - R^*\right\| \end{pmatrix}. \quad (32)$$

From Eq. (32) with $L_{\max,}$ it follows that,

$$\left\|Q(S_H, V_H, E_H, A_T, C_T, T_T, R) - \tau(S_H^*, V_H^*, E_H^*, A_A^*, C_T^*, T_T^*, R^*)\right\|.$$

$$\le \frac{\sigma(1-\phi) T_{\min^{\sigma-1}}}{AB(\phi)} L_{\max} \left\|Q(S_H, V_H, E_H, A_T, C_T, T_T, R) - (S_H^*, V_H^*, E_H^*, A_A^*, C_T^*, T_T^*, R^*)\right\|.$$

Therefore, Q is a contraction.

The proof establishes continuous and compact properties of P resulting in completely continuous status.

Then, it is satisfactory to establish that P is bounded and equicontinous.

Applying (B_2), it is observable that P is continuous as Q is also continuous.

consequently, for any $t \in \tau$, we obtained:

$$\left\|P_1 S_H\right\| \le \frac{\beta\sigma}{AB(\beta)\Gamma(\beta)} Sup_{t\in\tau}\left|\int_0^t S_H^{\sigma-1}(t-s)^{\phi-1} G_1\left(s, S_H(s)\right) ds\right|$$

$$\le \frac{\beta T^{\beta+\sigma-1}\Gamma(\sigma+1)}{AB(\beta)\Gamma(\beta+\sigma)}\left[g_{01}+g_{11}\left\|S_H\right\|+g_{21}\left\|V_H\right\|+g_{31}\left\|E_H\right\|+g_{41}\left\|A_T\right\|+g_{51}\left\|C_T\right\|+g_{61}\left\|T_T\right\|+g_{71}\left\|R\right\|\right]. \quad (33)$$

Then, P_1 is bounded.

Similarly, we have:

$$\left\|P_2 V_H\right\| \le \frac{\beta T^{\beta+\sigma-1}\Gamma(\sigma+1)}{AB(\beta)\Gamma(\beta+\sigma)}\left[g_{02}+g_{12}\left\|S_H\right\|+g_{22}\left\|V_H\right\|+g_{32}\left\|E_H\right\|+g_{42}\left\|A_T\right\|+g_{52}\left\|C_T\right\|+g_{62}\left\|T_T\right\|+g_{72}\left\|R\right\|\right],$$

$$\left\|P_3 E_H\right\| \le \frac{\beta T^{\beta+\sigma-1}\Gamma(\sigma+1)}{AB(\beta)\Gamma(\beta+\sigma)}\left[g_{02}+g_{12}\left\|S_H\right\|+g_{22}\left\|V_H\right\|+g_{32}\left\|E_H\right\|+g_{42}\left\|A_T\right\|+g_{52}\left\|C_T\right\|+g_{62}\left\|T_T\right\|+g_{72}\left\|R\right\|\right],$$

$$\left\|P_4 A_T\right\| \le \frac{\beta T^{\beta+\sigma-1}\Gamma(\sigma+1)}{AB(\beta)\Gamma(\beta+\sigma)}\left[g_{02}+g_{12}\left\|S_H\right\|+g_{22}\left\|V_H\right\|+g_{32}\left\|E_H\right\|+g_{42}\left\|A_T\right\|+g_{52}\left\|C_T\right\|+g_{62}\left\|T_T\right\|+g_{72}\left\|R\right\|\right],$$

$$\left\|P_5 C_T\right\| \le \frac{\beta T^{\beta+\sigma-1}\Gamma(\sigma+1)}{AB(\beta)\Gamma(\beta+\sigma)}\left[g_{02}+g_{12}\left\|S_H\right\|+g_{22}\left\|V_H\right\|+g_{32}\left\|E_H\right\|+g_{42}\left\|A_T\right\|+g_{52}\left\|C_T\right\|+g_{62}\left\|T_T\right\|+g_{72}\left\|R\right\|\right],$$

$$\left\|P_6 T_T\right\| \le \frac{\beta T^{\beta+\sigma-1}\Gamma(\sigma+1)}{AB(\beta)\Gamma(\beta+\sigma)}\left[g_{02}+g_{12}\left\|S_H\right\|+g_{22}\left\|V_H\right\|+g_{32}\left\|E_H\right\|+g_{42}\left\|A_T\right\|+g_{52}\left\|C_T\right\|+g_{62}\left\|T_T\right\|+g_{72}\left\|R\right\|\right],$$

$$\left\|P_7 R\right\| \le \frac{\beta T^{\beta+\sigma-1}\Gamma(\sigma+1)}{AB(\beta)\Gamma(\beta+\sigma)}\left[g_{02}+g_{12}\left\|S_H\right\|+g_{22}\left\|V_H\right\|+g_{32}\left\|E_H\right\|+g_{42}\left\|A_T\right\|+g_{52}\left\|C_T\right\|+g_{62}\left\|T_T\right\|+g_{72}\left\|R\right\|\right]. \quad (34)$$

Applying (33)-(34), and setting

$$\left\|P\right\| = \max\left\{\left\|P_1\right\|+\left\|P_2\right\|+\left\|P_3\right\|+\left\|P_4\right\|+\left\|P_5\right\|+\left\|P_6\right\|+\left\|P_7\right\|\right\}.$$

$$g_0^* = \max\left\{g_{0j}\right\}, g_1^* = \max\left\{g_{1j}\right\}, g_2^* = \max\left\{g_{2j}\right\}, g_3^* = \max\left\{g_{3j}\right\}, g_4^* = \max\left\{g_{4j}\right\}$$

With $g_5^* = \max\left\{g_{5j}\right\}, g_6^* = \max\left\{g_{6j}\right\}, g_7^* = \max\left\{g_{7j}\right\}$

$j = 1,2,3,...,7,$ it follows that,

$$\left\|P\left(S_H, V_H, E_H, A_T, C_T, A_T, R\right)\right\| \le \frac{\beta T^{\beta+\sigma-1}\Gamma(\sigma+1)}{AB(\beta)\Gamma(\beta+\sigma)}\left[\begin{matrix} g_0^*+g_1^*\left\|S_H\right\|+g_2^*\left\|V_H\right\|+g_3^*\left\|E_H\right\|+g_4^*\left\|A_T\right\| \\ +g_5^*\left\|C_T\right\|+g_6^*\left\|T_T\right\|+g_7^*\left\|R\right\| \end{matrix}\right].$$

(35)

This means that, P is bounded.

We have to show that, P is equicontinuity.

If, $t_1, t_2 \in \tau$ with $0 \le t_1 \le t_2 \in \tau$

We have,

$$\left|P_1 S_H(t_2) - P_1 S_H(t_1)\right| \le \frac{\beta\sigma}{AB(\beta)}\left|\int_0^{t_2} S^{\sigma-1}(t_2-s)^{\beta-1} ds - \int_0^{t_1} S_H^{\beta-1}(t_1-s)^{\beta-1} ds\right|.$$

$$\left|G_1\left(S_H, S_H(s)\right)\right| \le \frac{\beta\Gamma(\sigma+1)}{AB(\beta)\Gamma(\beta+\sigma)}\left|t_1^{\beta+\sigma-1} - t_2^{\beta+\sigma-1} + 2(t_2-t_1)^{\beta+\sigma-1} ds\right|\left[\begin{matrix} g_{01}+g_{11}\left\|S_H\right\|+g_{21}\left\|V_H\right\| \\ +g_{31}\left\|E_H\right\|+g_{41}\left\|A_T\right\|+g_{51}\left\|C_T\right\| \\ +g_{61}\left\|A_T\right\|+g_{71}\left\|R\right\| \end{matrix}\right],$$

$$\left|P_1\left(S_H, S_H(s)\right)\right| \le \frac{\beta\Gamma(\sigma+1)}{AB(\beta)\Gamma(\beta+\sigma)}\left|t_1^{\beta+\sigma-1} - t_2^{\beta+\sigma-1} + 2(t_2-t_1)^{\beta+\sigma-1} ds\right|\left[g_{01}+K_1\sum_{i=1}^{\infty} g_{i1}\right], \quad (36)$$

The right hand side of (36) is independent of $(S_H, V_H, E_H, A_T, C_T, T_T, R)$ The definition indicates that these quantities fulfill the three criteria of boundedness, uniform continuity and compactness so they are completely continuous.

Similarly, we have the following inequality;

$$\left|(P_2V_H)(t_2)-(P_2V_H)(t_1)\right| \le \frac{\beta\Gamma(\sigma+1)}{AB(\beta)\Gamma(\beta+\sigma)}\left|t_1^{\beta+\sigma-1}-t_2^{\beta+\sigma-1}+2(t_2-t_1)^{\beta+\sigma-1}ds\right|\left[g_{02}+K_2\sum_{i=1}^{\infty}g_{i2}\right],$$

$$\left|(P_3E_H)(t_2)-(P_3E_H)(t_1)\right| \le \frac{\beta\Gamma(\sigma+1)}{AB(\beta)\Gamma(\beta+\sigma)}\left|t_1^{\beta+\sigma-1}-t_2^{\beta+\sigma-1}+2(t_2-t_1)^{\beta+\sigma-1}ds\right|\left[g_{03}+K_3\sum_{i=1}^{\infty}g_{i3}\right],$$

$$\left|(P_4A_T)(t_2)-(P_4A_T)(t_1)\right| \le \frac{\beta\Gamma(\sigma+1)}{AB(\beta)\Gamma(\beta+\sigma)}\left|t_1^{\beta+\sigma-1}-t_2^{\beta+\sigma-1}+2(t_2-t_1)^{\beta+\sigma-1}ds\right|\left[g_{04}+K_4\sum_{i=1}^{\infty}g_{i4}\right],$$

$$\left|(P_5C_T)(t_2)-(P_5C_T)(t_1)\right| \le \frac{\beta\Gamma(\sigma+1)}{AB(\beta)\Gamma(\beta+\sigma)}\left|t_1^{\beta+\sigma-1}-t_2^{\beta+\sigma-1}+2(t_2-t_1)^{\beta+\sigma-1}ds\right|\left[g_{05}+K_5\sum_{i=1}^{\infty}g_{i5}\right],$$

$$\left|(P_6T_T)(t_2)-(P_6T_T)(t_1)\right| \le \frac{\beta\Gamma(\sigma+1)}{AB(\beta)\Gamma(\beta+\sigma)}\left|t_1^{\beta+\sigma-1}-t_2^{\beta+\sigma-1}+2(t_2-t_1)^{\beta+\sigma-1}ds\right|\left[g_{06}+K_6\sum_{i=1}^{\infty}g_{i6}\right],$$

$$\left|(P_7R)(t_2)-(P_7R)(t_1)\right| \le \frac{\beta\Gamma(\sigma+1)}{AB(\beta)\Gamma(\beta+\sigma)}\left|t_1^{\beta+\sigma-1}-t_2^{\beta+\sigma-1}+2(t_2-t_1)^{\beta+\sigma-1}ds\right|\left[g_{07}+K_7\sum_{i=1}^{\infty}g_{i7}\right]. \quad (37)$$

Similarly, the inequality from (36)-(37), that is

$$\left|Pi(S_H, V_H, E_H, A_T, C_T, T_T, R)(t_2)-Pi(S_H, V_H, E_H, A_T, C_T, T_T, R)(t_1)\right| \to 0 \; as t_2 \to t_1,$$

for i=1,2,3,...,7, this yields that, $Pi, i=1,2,3,...,7,$ Pi fulfills the requirements of being bounded, uniformly continuous and compact so it stands as completely continuous for $i=1,2,3,...7,$. By using Eq. (37) and making

$\|P\|$ with g_i^* for $j=0,1,2,...,7,$ we have

$$\left|Pi(S_H, V_H, E_H, A_T, C_T, T_T, R)(t_2)-Pi(S_H, V_H, E_H, A_T, C_T, T_T, R)(t_1)\right|$$

$$\le \frac{\beta\Gamma(\sigma+1)}{AB(\beta)\Gamma(\beta+\sigma)}\left|t_1^{\beta+\sigma-1}-t_2^{\beta+\sigma-1}+2(t_2-t_1)^{\beta+\sigma-1}ds\right|\left[g_{0i}^*+K_2\sum_{i=1}^{\infty}g_i^*\right].$$

(38)

The conditions of boundedness together with uniform continuity and compactness outline that P represents a completely continuous operator. Therefore, P satisfies the criteria for having at least one solution.

3.8 Numerical Scheme for the FF- Tuberculosis model

The second-order Adams-Bashforth algorithm will be used to create numerical solutions for FF- FF-Tuberculosis model (8).

We rewrite these integral equations (19), at $t=t_{n+1},$ this yields;

$$S_H(t_{n+1}) = S_{H0} + \sigma(1-\beta)t_n^{\sigma-1}G_1(t_n, S_H(t_n)) + \frac{\beta\sigma}{AB(\beta)\Gamma(\beta)}\int_0^{t+1}(t_{n+1}-s)^{\beta-1}S_H^{\sigma-1}G_1(s, S_H(s))ds,$$

$$V_H(t_{n+1}) = V_{H0} + \sigma(1-\beta)t_n^{\sigma-1}G_2(t_n, V_H(t_n)) + \frac{\beta\sigma}{AB(\beta)\Gamma(\beta)}\int_0^{t+1}(t_{n+1}-s)^{\beta-1}V_H^{\sigma-1}G_2(s, V_H(s))ds,$$

$$E_H(t_{n+1}) = E_{H0} + \sigma(1-\beta)t_n^{\sigma-1}G_3(t_n, E_H(t_n)) + \frac{\beta\sigma}{AB(\beta)\Gamma(\beta)}\int_0^{t+1}(t_{n+1}-s)^{\beta-1}E_H^{\sigma-1}G_3(s, E_H(s))ds,$$

$$A_T(t_{n+1}) = A_{T0} + \sigma(1-\beta)t_n^{\sigma-1}G_4(t_n, A_T(t_n)) + \frac{\beta\sigma}{AB(\beta)\Gamma(\beta)}\int_0^{t+1}(t_{n+1}-s)^{\beta-1}A_T^{\sigma-1}G_4(s, A_T(s))ds,$$

$$C_T(t_{n+1}) = C_{T0} + \sigma(1-\beta)t_n^{\sigma-1}G_5(t_n, C_T(t_n)) + \frac{\beta\sigma}{AB(\beta)\Gamma(\beta)}\int_0^{t+1}(t_{n+1}-s)^{\beta-1}C_T^{\sigma-1}G_5(s, C_T(s))ds,$$

$$T_T(t_{n+1}) = T_{T0} + \sigma(1-\beta)t_n^{\sigma-1}G_6(t_n, T_T(t_n)) + \frac{\beta\sigma}{AB(\beta)\Gamma(\beta)}\int_0^{t+1}(t_{n+1}-s)^{\beta-1}T_T^{\sigma-1}G_6(s, T_T(s))ds,$$

$$R(t_{n+1}) = R_0 + \sigma(1-\beta)t_n^{\sigma-1}G_7(t_n, R(t_n)) + \frac{\beta\sigma}{AB(\beta)\Gamma(\beta)}\int_0^{t+1}(t_{n+1}-s)^{\beta-1}R^{\sigma-1}G_7(s, R(s))ds. \quad (39)$$

So the numerical approximation of the integral (39) is obtained as;

$$S_H(t_{n+1}) = S_{H0} + \frac{\sigma(1-\beta)t_n^{\sigma-1}G_1(t_n, S_H(t_n))}{AB(\beta)} + \frac{\beta\sigma}{AB(\beta)\Gamma(\beta)}\sum_{j=1}^{n}\int_{t_j}^{t_{j+1}}(t_{j+1}-s)^{\beta-1}S_H^{\sigma-1}G_1(t_n, S_H^j(s))ds,$$

$$V_H(t_{n+1}) = V_{H0} + \frac{\sigma(1-\beta)t_n^{\sigma-1}G_2(t_n, V_H(t_n))}{AB(\beta)} + \frac{\beta\sigma}{AB(\beta)\Gamma(\beta)}\sum_{j=1}^{n}\int_{t_j}^{t_{j+1}}(t_{j+1}-s)^{\beta-1}S_H^{\sigma-1}G_2(t_n, V_H^j(s))ds,$$

$$E_H(t_{n+1}) = E_{H0} + \frac{\sigma(1-\beta)t_n^{\sigma-1}G_3(t_n, E_H(t_n))}{AB(\beta)} + \frac{\beta\sigma}{AB(\beta)\Gamma(\beta)}\sum_{j=1}^{n}\int_{t_j}^{t_{j+1}}(t_{j+1}-s)^{\beta-1}S_H^{\sigma-1}G_3(t_n, E_H^j(s))ds,$$

$$A_T(t_{n+1}) = A_{T0} + \frac{\sigma(1-\beta)t_n^{\sigma-1}G_4(t_n, A_T(t_n))}{AB(\beta)} + \frac{\beta\sigma}{AB(\beta)\Gamma(\beta)}\sum_{j=1}^{n}\int_{t_j}^{t_{j+1}}(t_{j+1}-s)^{\beta-1}A_T^{\sigma-1}G_4(t_n, A_T^j(s))ds,$$

$$C_T(t_{n+1}) = C_{T0} + \frac{\sigma(1-\beta)t_n^{\sigma-1}G_5(t_n, C_T(t_n))}{AB(\beta)} + \frac{\beta\sigma}{AB(\beta)\Gamma(\beta)}\sum_{j=1}^{n}\int_{t_j}^{t_{j+1}}(t_{j+1}-s)^{\beta-1}C_T^{\sigma-1}G_5(t_n, C_T^j(s))ds,$$

$$T_T(t_{n+1}) = T_{T0} + \frac{\sigma(1-\beta)t_n^{\sigma-1}G_6(t_n, T_T(t_n))}{AB(\beta)} + \frac{\beta\sigma}{AB(\beta)\Gamma(\beta)}\sum_{j=1}^{n}\int_{t_j}^{t_{j+1}}(t_{j+1}-s)^{\beta-1}T_T^{\sigma-1}G_6(t_n, T_T^j(s))ds,$$

$$R(t_{n+1}) = R_0 + \frac{\sigma(1-\beta)t_n^{\sigma-1}G_7(t_n, R(t_n))}{AB(\beta)} + \frac{\beta\sigma}{AB(\beta)\Gamma(\beta)}\sum_{j=1}^{n}\int_{t_j}^{t_{j+1}}(t_{j+1}-s)^{\beta-1}R^{\sigma-1}G_7(t_n, R^j(s))ds. \quad (40)$$

Two step Langrange's interpolation polynomials with $\Delta t = t_{j+1} - t_j$ function as an estimate for the integrand functions on $\left[t_j, t_{j+1}\right]$.

Thus, we obtained:

$$S_H(t_{n+1}) = S_{H0} + \frac{\sigma(1-\beta)t_n^{\sigma-1}G_1(t_n, S_H(t_n))}{AB(\beta)} + \frac{\beta\sigma}{AB(\beta)\Gamma(\beta)}\sum_{j=1}^{n}\int_{t_j}^{t_{j+1}}(t_{j+1}-s)^{\beta-1}S_H^{\sigma-1}Z_j^S(s)ds,$$

$$V_H(t_{n+1}) = V_{H0} + \frac{\sigma(1-\beta)t_n^{\sigma-1}G_2(t_n, V_H(t_n))}{AB(\beta)} + \frac{\beta\sigma}{AB(\beta)\Gamma(\beta)}\sum_{j=1}^{n}\int_{t_j}^{t_{j+1}}(t_{j+1}-s)^{\beta-1}V_H^{\sigma-1}Z_j^S(s)ds,$$

$$E_H(t_{n+1}) = E_{H0} + \frac{\sigma(1-\beta)t_n^{\sigma-1}G_3(t_n, E_H(t_n))}{AB(\beta)} + \frac{\beta\sigma}{AB(\beta)\Gamma(\beta)}\sum_{j=1}^{n}\int_{t_j}^{t_{j+1}}(t_{j+1}-s)^{\beta-1}E_H^{\sigma-1}Z_j^S(s)ds,$$

$$A_T(t_{n+1}) = A_{T0} + \frac{\sigma(1-\beta)t_n^{\sigma-1}G_4(t_n, A_T(t_n))}{AB(\beta)} + \frac{\beta\sigma}{AB(\beta)\Gamma(\beta)}\sum_{j=1}^{n}\int_{t_j}^{t_{j+1}}(t_{j+1}-s)^{\beta-1}A_T^{\sigma-1}Z_j^S(s)ds,$$

$$C_T(t_{n+1}) = C_{T0} + \frac{\sigma(1-\beta)t_n^{\sigma-1}G_5(t_n, C_T(t_n))}{AB(\beta)} + \frac{\beta\sigma}{AB(\beta)\Gamma(\beta)}\sum_{j=1}^{n}\int_{t_j}^{t_{j+1}}(t_{j+1}-s)^{\beta-1}C_T^{\sigma-1}Z_j^S(s)ds,$$

$$T_T(t_{n+1}) = T_{T0} + \frac{\sigma(1-\beta)t_n^{\sigma-1}G_6(t_n, T_T(t_n))}{AB(\beta)} + \frac{\beta\sigma}{AB(\beta)\Gamma(\beta)}\sum_{j=1}^{n}\int_{t_j}^{t_{j+1}}(t_{j+1}-s)^{\beta-1}T_T^{\sigma-1}Z_j^S(s)ds,$$

$$R(t_{n+1}) = R_0 + \frac{\sigma(1-\beta)t_n^{\sigma-1}G_7(t_n, R(t_n))}{AB(\beta)} + \frac{\beta\sigma}{AB(\beta)\Gamma(\beta)}\sum_{j=1}^{n}\int_{t_j}^{t_{j+1}}(t_{j+1}-s)^{\beta-1}R^{\sigma-1}Z_j^S(s)ds, \quad (41)$$

Where,

$$Z_j^{S_H}(s) = \frac{s-t_{j-1}}{t_j-t_{j-1}}t_j^{\sigma-1}G_1(s, S_H^j(s)) - \frac{s-t_{j-1}}{t_j-t_{j-1}}t_{j-1}^{\sigma-1}G_1(s, S_H^{j-1}(s)),$$

$$Z_j^{V_H}(s) = \frac{s-t_{j-1}}{t_j-t_{j-1}}t_j^{\sigma-1}G_2(s, V_H^j(s)) - \frac{s-t_{j-1}}{t_j-t_{j-1}}t_{j-1}^{\sigma-1}G_2(s, V_H^{j-1}(s)),$$

$$Z_j^{E_H}(s) = \frac{s-t_{j-1}}{t_j-t_{j-1}}t_j^{\sigma-1}G_3(s, E_H^j(s)) - \frac{s-t_{j-1}}{t_j-t_{j-1}}t_{j-1}^{\sigma-1}G_3(s, E_H^{j-1}(s)),$$

$$Z_j^{A_T}(s) = \frac{s-t_{j-1}}{t_j-t_{j-1}}t_j^{\sigma-1}G_4(s, A_T^j(s)) - \frac{s-t_{j-1}}{t_j-t_{j-1}}t_{j-1}^{\sigma-1}G_4(s, A_T^{j-1}(s)),$$

$$Z_j^{C_T}(s) = \frac{s-t_{j-1}}{t_j-t_{j-1}}t_j^{\sigma-1}G_5(s, C_T^j(s)) - \frac{s-t_{j-1}}{t_j-t_{j-1}}t_{j-1}^{\sigma-1}G_5(s, C_T^{j-1}(s)),$$

$$Z_j^{T_T}(s) = \frac{s-t_{j-1}}{t_j-t_{j-1}}t_j^{\sigma-1}G_6(s, T_T^j(s)) - \frac{s-t_{j-1}}{t_j-t_{j-1}}t_{j-1}^{\sigma-1}G_6(s, T_T^{j-1}(s)),$$

$$Z_j^{R}(s) = \frac{s-t_{j-1}}{t_j-t_{j-1}}t_j^{\sigma-1}G_7(s, R^j(s)) - \frac{s-t_{j-1}}{t_j-t_{j-1}}t_{j-1}^{\sigma-1}G_7(s, T^{j-1}(s)), \quad (42)$$

We finally solved the schemes needed for numerical calculations of the FF-Tuberculosis model (8).

$$S_H(t_{n+1}) = S_{H0} + \sigma(1-\beta)t_n^{\sigma-1}G_1(t_n, S_H(t_n)) + \frac{\sigma(\Delta t)^\beta}{AB(\beta)\Gamma(\beta+2)}\sum_{j=1}^{n}\begin{bmatrix} t_j^{\sigma-1}G_1(s, S_H^j(s))X_1(n,j) \\ -t_{j-1}^{\sigma-1}G_1(s, S_H^{j-1}(s))X_2(n,j)\end{bmatrix},$$

$$V_H(t_{n+1}) = V_{H0} + \sigma(1-\beta)t_n^{\sigma-1}G_2(t_n, V_H(t_n)) + \frac{\sigma(\Delta t)^\beta}{AB(\beta)\Gamma(\beta+2)}\sum_{j=1}^{n}\begin{bmatrix} t_j^{\sigma-1}G_2(s, V_H^j(s))X_1(n,j) \\ -t_{j-1}^{\sigma-1}G_2(s, V_H^{j-1}(s))X_2(n,j)\end{bmatrix},$$

$$E_H(t_{n+1}) = E_{H0} + \sigma(1-\beta)t_n^{\sigma-1}G_3(t_n, E_H(t_n)) + \frac{\sigma(\Delta t)^\beta}{AB(\beta)\Gamma(\beta+2)}\sum_{j=1}^{n}\begin{bmatrix} t_j^{\sigma-1}G_3(s, E_H^j(s))X_1(n,j) \\ -t_{j-1}^{\sigma-1}G_3(s, E_H^{j-1}(s))X_2(n,j)\end{bmatrix},$$

$$A_T(t_{n+1}) = A_{T0} + \sigma(1-\beta)t_n^{\sigma-1}G_4(t_n, A_T(t_n)) + \frac{\sigma(\Delta t)^\beta}{AB(\beta)\Gamma(\beta+2)}\sum_{j=1}^{n}\begin{bmatrix} t_j^{\sigma-1}G_4(s, A_T^j(s))X_1(n,j) \\ -t_{j-1}^{\sigma-1}G_4(s, A_T^{j-1}(s))X_2(n,j)\end{bmatrix},$$

$$C_T(t_{n+1}) = C_{T0} + \sigma(1-\beta)t_n^{\sigma-1}G_5(t_n, C_T(t_n)) + \frac{\sigma(\Delta t)^\beta}{AB(\beta)\Gamma(\beta+2)}\sum_{j=1}^{n}\begin{bmatrix} t_j^{\sigma-1}G_5(s, C_T^j(s))X_1(n,j) \\ -t_{j-1}^{\sigma-1}G_5(s, C_T^{j-1}(s))X_2(n,j)\end{bmatrix},$$

$$T_T\left(t_{n+1}\right)=T_{T0}+\sigma\left(1-\beta\right)t_n^{\sigma-1}G_6\left(t_n,T_T\left(t_n\right)\right)+\frac{\sigma\left(\Delta t\right)^{\beta}}{AB\left(\beta\right)\Gamma\left(\beta+2\right)}\sum_{j=1}^{n}\begin{bmatrix}t_j^{\sigma-1}G_6\left(s,T_T^{j}\left(s\right)\right)X_1\left(n,j\right)\\-t_{j-1}^{\sigma-1}G_6\left(s,T_T^{j-1}\left(s\right)\right)X_2\left(n,j\right)\end{bmatrix},$$

$$R\left(t_{n+1}\right)=R_0+\sigma\left(1-\beta\right)t_n^{\sigma-1}G_7\left(t_n,R\left(t_n\right)\right)+\frac{\sigma\left(\Delta t\right)^{\beta}}{AB\left(\beta\right)\Gamma\left(\beta+2\right)}\sum_{j=1}^{n}\begin{bmatrix}t_j^{\sigma-1}G_7\left(s,R^{j}\left(s\right)\right)X_1\left(n,j\right)\\-t_{j-1}^{\sigma-1}G_7\left(s,R^{j-1}\left(s\right)\right)X_2\left(n,j\right)\end{bmatrix}. \quad (43)$$

Where

$$X_1\left(n,j\right)=\left(n+1-j\right)^{\phi+1}-\left(n-j\right)^{\phi}-\left(n-j\right)^{\phi}\left(n-j+2+2\phi\right) \quad (44)$$

And $X_2\left(n,j\right)=\left(n+1-j\right)^{\phi+1}-\left(n-j\right)^{\phi}-\left(n-j\right)^{\phi}\left(n-j+1+\phi\right).$

The number of confirmed tuberculosis cases reported each year from 2014 to 2021 is outlined in Table 2.

Table 2. Trends in confirmed Tuberculosis cases, 2014–2021.

Year	Cases
2014	550,000
2015	650,000
2016	750,000
2017	800,000
2018	900,000
2019	1,000,000
2020	1,250,000
2021	1,100,000

Source. Authors' adaptation based on *Agbata et al.* (2025a, 2025b).

3.9 Data Fitting

To match the collected data with the mathematical models for malaria and tuberculosis, we used the fmincon function in MATLAB's Optimization Toolbox (Duru et al., 2024; Ugwu et al., 2020). This tool helps fine-tune the parameters so that the model outcomes line up more closely with what is actually seen in the real world. By narrowing the gap between predicted and observed values, the process improves the model's accuracy and reliability. The fitted results are shown in the following figures (Agbata et al., 2025a), where the side-by-side comparison highlights how well the model reflects the reported case data.

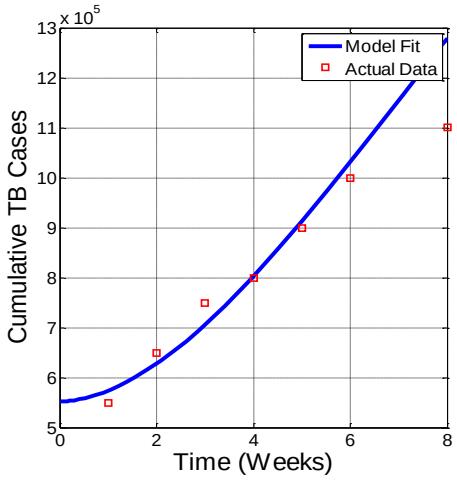

Figure 2b. Data fitting for the TB model

Figure 2b illustrates the fitting of the TB model to real case data, displaying a comparison between simulated projections and reported tuberculosis incidence over the study period (Agbata et al., 2024b; Bolaji et al., 2024). The plot generally features a line representing model estimates alongside discrete points corresponding to observed data (Acheneje et al., 2024; Agbata et al., 2024a). A strong overlap between these elements reflects a reliable fit, indicating that the model effectively reproduces the transmission dynamics of TB.

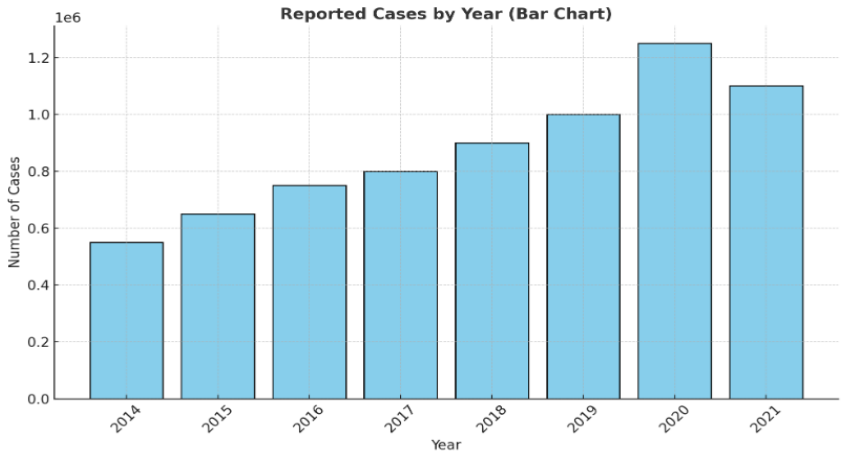

Figure 2c. Bar chart representing reported cases

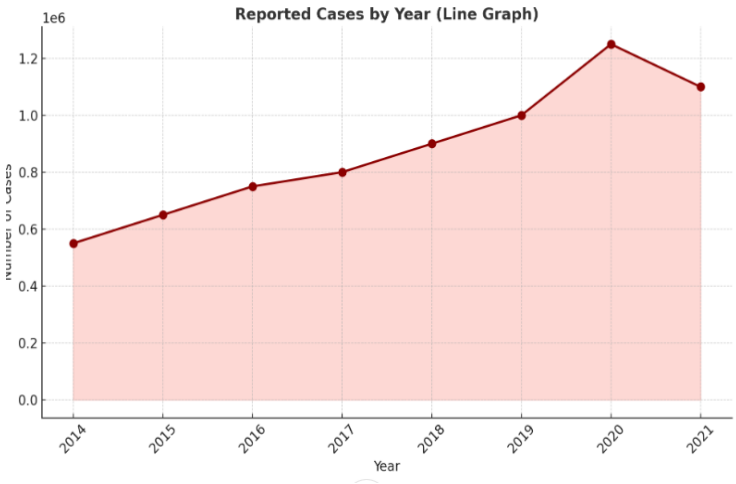

Figure 2d. Line graph representing reported cases

Figures 2c and 2d illustrate the temporal dynamics of reported cases from 2014 to 2021. Both figures reveal a steady increase in cases from 2014 through 2019, followed by a sharp rise in 2020 and then a decline in 2021. Epidemiologically, this trend suggests an expanding burden of disease over several years, possibly reflecting ongoing transmission, improved detection, or both, until 2019 (Duru et al., 2024; Ugwu et al., 2020). The peak observed in 2020 may indicate an outbreak year, amplified transmission, or changes in surveillance and reporting systems (Agbata et al., 2025a). The decline in 2021, while notable, does not return to pre-2019 levels, suggesting that although transmission may have slowed, the disease burden remains high. From a quantitative perspective, model fitting of a linear trend to the data produced a mean squared error (MSE) of approximately 22.66×10^9 and a coefficient of determination (R^2) of 0.932. The high R^2 indicates that the linear trend explains more than 93% of the variation in reported cases, while the relatively large MSE reflects deviations introduced by the sharp peak in 2020. This highlights the epidemiological reality that outbreaks often follow nonlinear dynamics due to sudden shifts in transmission drivers, such as behavioral changes, environmental factors, or intervention coverage. The bar and line plots emphasize both the long-term upward trajectory and the short-term fluctuations in reported cases, highlighting the need for sustained public health measures to control transmission while remaining vigilant for outbreak surges.

4. Simulation and Discussion

Running simulations of disease models with specified parameter values plays a crucial role in exploring how infections such as malaria or tuberculosis propagate within communities (Anyanwu & Mbah, 2021; Collins & Duffy, 2022; Mishra & Aldosari, 2025). The resulting visual outputs allow researchers and health authorities to assess how different factors and interventions influence transmission patterns. Such analyses illustrate potential disease trajectories under varying conditions and support evidence-based decisions on effective control or elimination strategies (Atokolo & Mbah, 2020; Odeh et al., 2024). In essence, these simulations transform complex epidemiological data into practical insights that can guide public health planning and improve population health outcomes.

Table 3. Parameters values used for simulations.

Parameter	Values	Sources
Λ_H	0.00011	Agbata et al. (2025a)
β_T	0.334	Fitted
K_T	0.8333	Agbata et al. (2025a)
θ_T	0.45	Fitted
μ_H	0.00004	Agbata et al. (2025a)
γ_T	0.62	Fitted
τ	0.001000	Fitted
δ_T	0.10000	Fitted,
α_T	0.76000	Fitted
ω	0.8000	Agbata et al. (2025a)
σ_T	0.600	Agbata et al. (2025a)
ψ_T	0.200	Agbata et al. (2025a)

Table 3 gives the parameter values used in simulations of the TB model, serving as the numerical basis for simulations and analyses (Agbata et al., 2025a). It also distinguishes between parameters that remain constant and those that can be adjusted for sensitivity testing or scenario evaluation.

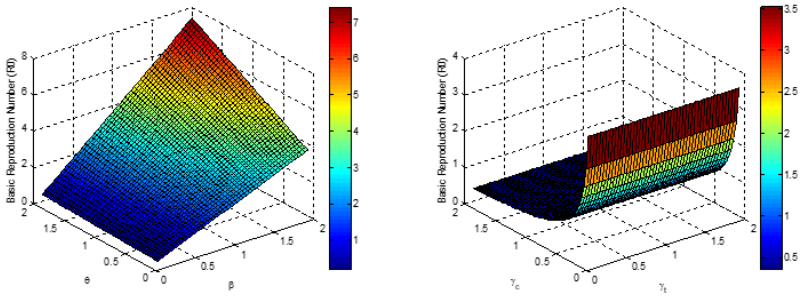

(b) Impact of θ and β on R_0^T (a) Impact of γ_c and γ_T on R_0^T

Figure 3. Surface plot of the basic reproduction number

Figure 3(a) shows that as the progression rate from exposed to infected individuals and the contact rate between susceptible and infected individuals increase, the basic reproduction number R_0 for tuberculosis also rises, surpassing one. This suggests that overlooking these parameters could significantly intensify the spread of tuberculosis within the population. In contrast, Figure 3(b) presents a surface plot illustrating the influence of treatment rates for both acutely and chronically infected individuals on R_0. The results indicate that while R_0 initially increases with higher treatment rates, it remains below one, underscoring that strengthening treatment interventions can substantially mitigate the impact of tuberculosis in the population.

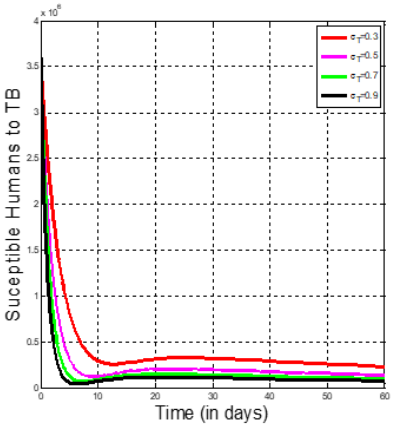

(b) Simulation of Susceptible Humans to Tuberculosis

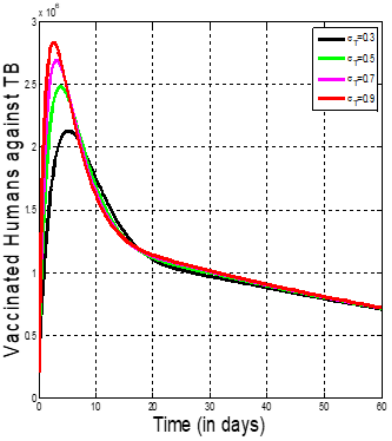

(a) Simulation of Vaccinated Humans to Tuberculosis

Figure 4. Effect of σ_T on $S_H(t)$ and $V_H(t)$

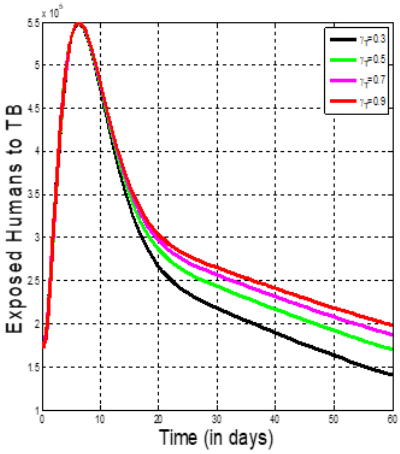

(a) Simulation of Exposed Humans to Tuberculosis

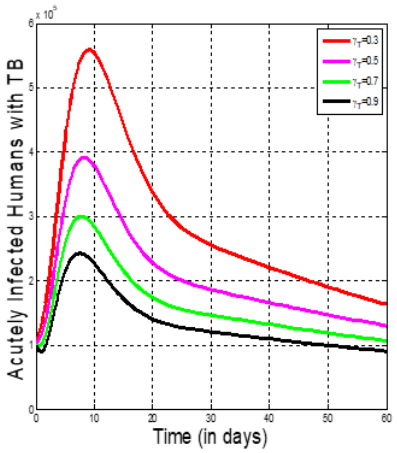

(b) Simulation of Acutely infected Humans to Tuberculosis

Figure 5. Effect of γ_T on $E_H(t)$ and $A_T(t)$

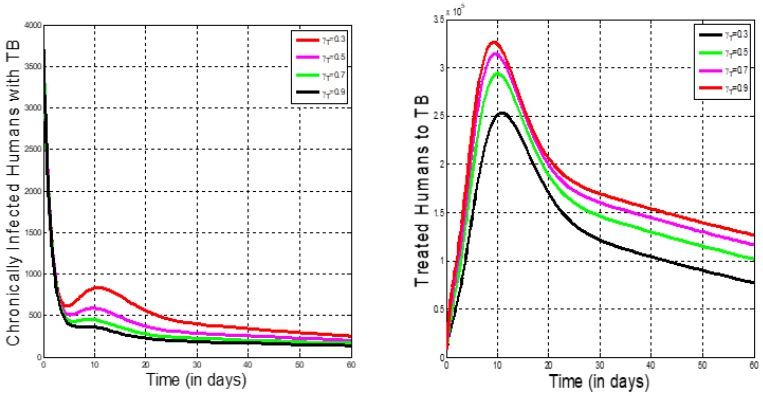

(a) Simulation of Chronically infected Humans to

(b) Simulation of Treated Humans to Tuberculosis

Figure 6. Effect of γ_T on $C_T(t)$ Populatin $T_T(t)$

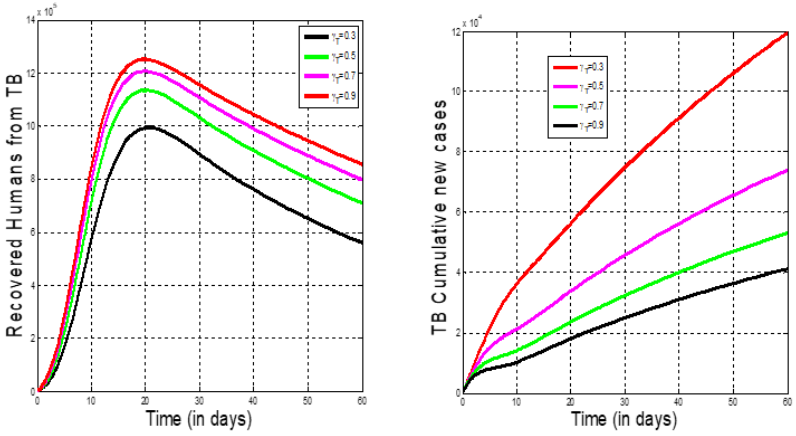

(a) Simulation of Recovered Humans from Tuberculosis

(b) Simulation of Tuberculosis Cumulative new cases

Figure 7. Effect of γ_T on $R(t)$ and Cumulative new cases

Fig 4a shows the susceptible population beginning at approximately 3.5×10^6 individuals across all vaccination rate scenarios and experiencing a rapid decline during the initial 20 days of simulation. This sharp decrease represents individuals transitioning out of the susceptible compartment primarily through vaccination, with some also becoming infected with tuberculosis. Higher vaccination rates σ_T produce steeper declines and result in lower steady-state levels of susceptible individuals. After the initial transition period, each scenario reaches an equilibrium where the susceptible population stabilizes at different levels depending on the vaccination rate employed, demonstrating the

effectiveness of vaccination programs in reducing the pool of individuals at risk for tuberculosis infection.

Fig 4b demonstrates the vaccinated population starting from zero and showing a rapid increase during the first 20 days, reaching distinct peak levels that correspond directly to the vaccination rate parameter σ_T. Higher vaccination rates produce higher peak vaccinated populations, demonstrating the immediate impact of intensive vaccination efforts. Following these peaks, all scenarios exhibit a gradual decline in the vaccinated population over time, which reflects waning vaccine immunity, movement of individuals to other epidemiological compartments, or reduced vaccination rates as fewer susceptible individuals remain available for vaccination. The timing and magnitude of both the peak and subsequent decline are directly influenced by the vaccination rate, indicating that sustained vaccination efforts may be necessary to maintain population-level protection against tuberculosis. Fig 5a shows the exposed human population beginning at approximately 6×10^6 individuals and exhibiting a rapid peak within the first few days before declining exponentially over time. The different colored lines represent varying treatment rates of infected individuals γ_T, demonstrating that higher treatment rates produce steeper declines and lower steady-state levels of exposed individuals. This pattern occurs because treating infected individuals more effectively reduces their infectiousness and transmission capacity, thereby decreasing the rate at which susceptible individuals become exposed to tuberculosis. The exponential decline indicates that as fewer infected individuals remain untreated in the population, the exposure risk diminishes significantly, leading to a sustained reduction in the exposed compartment over the simulation period. Fig 5b demonstrates the acutely infected population starting near zero and rapidly increasing to peak levels around 5×10^6 individuals within the first 10 days, then gradually declining over the remaining time period. Higher treatment rates of infected individuals γ_T result in faster declines and lower equilibrium levels of acutely infected people. This direct relationship demonstrates that increasing the treatment rate of infected individuals accelerates their recovery or removal from the infectious pool, thereby reducing the overall burden of acute tuberculosis infection in the population. The initial rise represents individuals progressing from exposed to acutely infected status, while the subsequent decline reflects the combined effects of treatment interventions and natural disease progression.

Fig 6a shows the chronically infected population beginning at a low baseline level around 0-500 individuals and remaining relatively stable throughout the simulation period across all treatment rate scenarios. Unlike the acute infection dynamics, the chronically infected compartment shows minimal variation with changes in the treatment rate of infected individuals γ_T, with different colored lines representing various γ_T values remaining closely clustered. This pattern indicates that treatment rate variations have limited impact on chronically infected population size, suggesting that individuals in chronic infection stages may be less responsive to standard treatment interventions due to drug resistance, treatment complications, or the persistent nature of chronic tuberculosis infection. Fig 6b shows the treated population starting near zero and rapidly increasing to peak levels around 3.4×10^6 individuals within the first 10-15 days, then gradually declining over the simulation period. Higher treatment rates of infected individuals γ_T produce higher peak levels and more sustained treated populations, as indicated by the different colored lines. The initial rapid rise reflects immediate implementation of treatment programs for infected individuals, while the subsequent decline represents individuals completing treatment and transitioning out through recovery. The direct relationship between γ_T and both peak height and sustained levels demonstrates that increasing treatment rates effectively moves more infected individuals into treatment, leading to better population-level tuberculosis control.

Fig 7a shows the recovered human population starting from zero and steadily increasing over the simulation period, with all scenarios reaching peak levels around 12×10^5 individuals before showing slight declines in the later stages. Higher treatment rates of infected individuals γ_T produce higher peak recovery levels and more sustained recovery populations, as indicated by the different colored lines. The initial gradual rise reflects individuals successfully completing treatment and transitioning from infected to recovered status. The peak occurs when the recovery rate is maximized relative to new infections, while the subsequent slight decline may represent the depletion of the infected pool available for treatment or possible re-infection of recovered individuals. The direct relationship between γ_T and recovery levels demonstrates that increasing treatment rates effectively enhances population-level recovery from tuberculosis. Fig 7b demonstrates the tuberculosis cumulative new cases starting from zero and showing continuous linear increases throughout the simulation period, with different treatment rates producing distinctly different cumulative case trajectories. Lower treatment rates of infected individuals γ_T result in steeper slopes and higher cumulative case counts, while higher treatment rates produce more gradual increases and lower total case accumulation. The linear nature of these curves indicates a constant rate of new case generation over time, with the slope directly influenced by the treatment rate parameter. This pattern shows that higher treatment rates effectively reduce the rate of new tuberculosis case development by decreasing transmission from infected individuals, demonstrating the critical importance of prompt and effective treatment in controlling tuberculosis spread at the population level.

5. Conclusion

This study presents a fractal–fractional deterministic model for tuberculosis (TB) that integrates vaccination, treatment interventions, waning immunity, and environmental measures into a seven-compartment framework. By employing fractal–fractional derivatives with Mittag–Leffler kernels, the model advanced beyond classical integer-order approaches by embedding memory and hereditary properties into the disease dynamics. These features provided a more accurate representation of TB's latent progression, prolonged infectious periods, and the delayed impact of interventions. Theoretical analysis established the positivity, boundedness, and biological feasibility of the model, ensuring that solutions remain epidemiologically valid. The disease-free and endemic equilibrium points were derived, and the basic reproduction number (R_0) was calculated to serve as a threshold parameter for TB persistence. Sensitivity analysis demonstrated that parameters such as contact rate and progression from exposure to active infection amplify R_0, while treatment, vaccination, and environmental interventions reduce it. These findings indicate that biomedical and environmental strategies must be implemented simultaneously to sustainably suppress TB transmission. Numerical simulations using the Adams–Bashforth scheme confirmed the analytical results. Vaccination led to a rapid reduction in the susceptible pool and increased the vaccinated population, while treatment significantly reduced acute and chronic infections. Environmental interventions contributed to lowering transmission through improved living and ventilation conditions. Model fitting with WHO incidence data showed strong agreement, confirming the model's predictive reliability. These outcomes emphasized that integrated intervention approaches are more effective than single strategies, highlighting the importance of combining medical treatment with preventive and environmental measures.

Future studies should consider spatial heterogeneity, drug-resistant strains, and TB co-infections, while also applying stochastic methods and economic evaluations. Broader multi-regional data validation will strengthen the model's predictive value for global TB control.

6. Availability of Data

The data used in this study are obtained National Centre for Disease Control (NCDC) and others obtained from existing literature are presented and referenced in table 2 of this manuscript. The data and source codes used for simulation are available from the corresponding and lead author on reasonable request.

7. AI Use Statement

The author(s) declare that no artificial intelligence tools were used in the preparation, writing, analysis, or editing of this manuscript. The content of the manuscript was prepared entirely by the author(s).

References

Abdo, M. S., Alghamdi, N., Alzumi, H. Z., & Shammakh, W. (2025). Fractional-order modeling of tuberculosis and diabetes mellitus co-existence dynamics. Computers in Biology and Medicine, 195, 110514. https://doi.org/10.1016/j.compbiomed.2025.110514

Acheneje, G. O., Omale, D., Agbata, B. C., Atokolo, W., Shior, M. M., & Bolawarinwa, B. (2024). Approximate solution of the fractional order mathematical model on the transmission dynamics of the co-infection of COVID-19 and Monkeypox using the Laplace-Adomian decomposition method. International Journal of Mathematics and Statistics Studies, 12(3), 17–51. https://eajournals.org/ijmss/vol12issue-3

Adepoju, V. A., Adesola, A. A., & Abioye, A. I. (2020). Factors influencing tuberculosis case detection in Nigeria: A systematic review. Pan African Medical Journal, 36, 89. https://doi.org/10.11604/pamj.2020.36.89.22364

Adejumo, O. A., Daniel, O. J., Adebayo, B. I., Adejumo, E. N., Jaiyesimi, E. O., Akang, G., & Otesanya, A. F. (2016). Childhood tuberculosis in Nigeria: Disease presentation and treatment outcomes. Health Science Reports, 1(10), e28. https://doi.org/10.1002/hsr2.28

Agbata, B. C., Agbebaku, D. F., Odo, C. E., Ojih, J. T., Shior, M. M., & Ezugorie, I. G. (2024). A mathematical model for the transmission dynamics of COVID-19 in Nigeria and its post-effects. International Journal of Mathematical Analysis and Modelling, 7(2), 523–547. https://tnsmb.org/journal/index.php/ijmam/article/view/191

Agbata, B. C., Cenaj, E., Agbebaku, D. F., Collins, O. C., Dervishi, R., Emadifar, H., Ezeafulukwe, A. U., & Mbah, G. C. E. (2025b). Mathematical analysis of the transmission dynamics of malaria and tuberculosis co-infection with control strategies. Engineering Reports, 7(6), e70210. https://doi.org/10.1002/eng2.70210

Agbata, B. C., Dervishi, R., Agbebaku, D. F., Cenaj, E., Collins, O. C., Ezeafulukwe, A. U., Shior, M.-A., & Mbah, G. C. E. (2025c). A comprehensive analysis of fractional-order model of tuberculosis with treatment intervention. BMC Infectious Diseases, 25, 1070. https://doi.org/10.1186/s12879-025-11303-9

Agbata, B. C., Obeng-Denteh, W., Amoah-Mensah, J., Kwabi, P. A., Shior, M. M., Asante-Mensa, F., & Abraham, S. (2024). Numerical solution of fractional order model of measles disease with double dose vaccination. Dutse Journal of Pure and Applied Sciences (DUJOPAS), 10(3b), 202–217. https://www.ajol.info/index.php/dujopas/article/view/281624

Agbata, C. B., Meco, Z. M., Agbebaku, D. F., Dervishi, R., & Ezike, M. G. C. (2025a). Fractional-order analysis of malaria and tuberculosis co-dynamics: A Laplace Adomian decomposition approach. Edelweiss Applied Science and Technology, 9(4), 1675–1714. https://doi.org/10.55214/25768484.v9i4.6353

Akowe, E., Ahman, Q. O., Agbata, B. C., Joseph, S. O., Senewo, E. O., Danjuma, A. Y., & Yahaya, D. J. (2025). A novel malaria mathematical model: Integrating vector and non-vector transmission pathways. BMC Infectious Diseases, 25, Article 322. https://doi.org/10.1186/s12879-025-10653-8

Anyanwu, M. C., & Mbah, G. C. E. (2021). Stability analysis of a mathematical model for the use of Wolbachia to stop the spread of Zika virus disease. Biometrical Letters, 58(1), 41–58. https://doi.org/10.2478/bile-2021-0003

Atangana, A., Akgu, A., & Owolabi, K. M. (2020). Analysis of fractal fractional differential equations. Alexandria Engineering Journal, 59(3), 1117–1134. https://doi.org/10.1016/j.aej.2020.01.005

Atokolo, W., & Mbah, G. C. E. (2020). Modeling the control of Zika virus vector population using the sterile insect technology. Journal of Applied Mathematics, 2020, Article 6350134. https://doi.org/10.1155/2020/6350134

Avazzadeh, Z., Hassani, H., Agarwal, P., Mehrabi, S., Ebadi, M. J., & Dahaghin, M. S. (2023). An optimization method for studying fractional-order tuberculosis disease model via generalized Laguerre polynomials. Soft Computing, 27(49), 9519–9531. https://doi.org/10.1007/s00500-023-08086-z

Balogun, M., Sekoni, A., Meloni, S. T., Odukoya, O. O., Onajole, A., & Kanki, P. (2020). A systematic review and meta-analysis of tuberculosis and HIV co-infection in Nigeria. PLoS ONE, 15(3), e0230321. https://doi.org/10.1371/journal.pone.0230321

Barry, M., Al Amri, M., Memish, Z. A., & Zumla, A. (2021). Prevalence of latent tuberculosis infection in the Middle East and North Africa: A systematic review. BMC Public Health, 21(1), 956. https://doi.org/10.1186/s12889-021-10928-5

Bolaji, B., Onoja, T., Agbata, B. C., Omede, B. I., & Odionyenma, U. B. (2024). Dynamical analysis of HIV-TB co-infection transmission model in the presence of treatment for TB. Bulletin of Biomathematics, 2(1), 21–56. https://doi.org/10.59292/bulletinbiomath.2024002

Cohen, A., Mathiasen, V. D., Schön, T., & Wejse, C. (2019). The global prevalence of latent tuberculosis: A systematic review and meta-analysis. European Respiratory Journal, 54(3). https://doi.org/10.1183/13993003.00655-2019

Collins, O. C., & Duffy, K. J. (2022). A mathematical model for the dynamics and control of malaria in Nigeria. Infectious Disease Modelling, 7(4), 728–741. https://doi.org/10.1016/j.idm.2022.10.005

Daniel, O. J., Oladapo, O. T., Alausa, O. K., & Ogunniyi, A. (2006). Prevalence of tuberculosis among HIV/AIDS patients in Nigeria: A cross-sectional study. Journal of the National Medical Association, 98(6), 862–865.

Duru, E. C., Mbah, G. C. E., Anyanwu, M. C., & Topman, N. N. (2024). Modelling the co-infection of malaria and Zika virus disease. Journal of the Nigerian Society of Physical Sciences. Advance online publication. https://doi.org/10.46481/jnsps.2024.1938

El Baz, O., Khaloufi, I., Kouidere, A., Laarabi, H., & Rachik, M. (2024). Analysis and optimal control problem for a fractional mathematical model of tuberculosis with smoking consideration. Mathematical Modeling and Computing, 11(2), 492–504. https://doi.org/10.23939/mmc2024.02.492

Eshetie, S., Gizachew, M., Dagnew, M., Kumera, G., Woldie, H., Ambaw, F., & Moges, F. (2018). Multidrug-resistant tuberculosis in Ethiopian settings: A systematic review and meta-analysis. BMC Infectious Diseases, 18(1), 486. https://doi.org/10.1186/s12879-018-3385-6

Granas, A., & Dugundji, J. (2003). Fixed point theory. Springer. https://doi.org/10.1007/978-0-387-21593-8

Khan, A., Shah, K., Abdeljawad, T., & Amacha, I. (2024). Fractal fractional model for tuberculosis: Existence and numerical solutions. Scientific Reports, 14, 12211. https://doi.org/10.1038/s41598-024-62386-4

Krasnosel'skii, M. A. (1955). Two remarks on the method of successive approximations. Uspekhi Matematicheskikh Nauk, 10, 123–127.

Mishra, M. N., & Aldosari, F. (2025). Comparative study of tuberculosis infection by using general fractional derivative. AIMS Mathematics, 10(1), 1224–1247. https://doi.org/10.3934/math.2025058

Nandi, T. R., Saha, A. K., & Roy, S. (2024). Analysis of a fractional order epidemiological model for tuberculosis transmission with vaccination and reinfection. Scientific Reports, 14, 28290. https://doi.org/10.1038/s41598-024-73392-x

Odeh, J. O., Agbata, B. C., Ezeafulukwe, A. U., Madubueze, C. E., Acheneje, G. O., & Topman, N. N. (2024). A mathematical model for the control of chlamydia disease with treatment strategy. Journal of Mathematical Acumen and Research, 7(1), 45–60. https://www.researchgate.net/publication/381278254

Olusoji, D., & Hassan, A. (2018). Prevalence and pattern of multidrug-resistant tuberculosis in Oyo State, Nigeria. Annals of African Medicine, 17(2), 59–65. https://doi.org/10.4103/aam.aam_15_17

Qureshi, S., Atangana, A., & Shaikh, A. (2019). Strange chaotic attractors under fractal fractional operators using newly proposed numerical methods. The European Physical Journal Plus, 134, 13003. https://doi.org/10.1140/epjp/i2019-13003-7

Rahman, M. U. (2022). Generalized fractal-fractional order problems under non-singular Mittag-Leffler kernel. Results in Physics, 35, 105346. https://doi.org/10.1016/j.rinp.2022.105346

Ugwu, K. O., Onah, I. S., Mbah, G. C., & Ezeonu, I. M. (2020). Rifampicin resistance patterns and dynamics of tuberculosis and drug-resistant tuberculosis in Enugu, South Eastern Nigeria. Journal of Infection in Developing Countries, 14(9), 1011–1018. https://doi.org/10.3855/jidc.12736

World Health Organization. (2024). Global tuberculosis report 2024. Geneva, Switzerland: World Health Organization. https://www.who.int/teams/global-tuberculosis-programme/tb-reports/global-tuberculosis-report-2024/tb-disease-burden/1-1-tb-incidence

World Health Organization. (2025, March 24). WHO calls for immediate action as report shows 10% rise in child TB infections in European region. https://www.reuters.com/business/healthcare-pharmaceuticals/who-calls-immediate-action-report-shows-10-rise-child-tb-infections-european-2025-03-24/